Functional implementation of a linear glycolysis for sugar catabolism in Pseudomonas putida

Sánchez-Pascuala, Alberto; Fernandez-Cabezon, Lorena; de Lorenzo, Víctor; Nikel, Pablo Ivan

Published in:
Metabolic Engineering

Link to article, DOI:
10.1016/j.ymben.2019.04.005

Publication date:
2019

Document Version
Peer reviewed version

Functional implementation of a linear glycolysis for sugar catabolism in *Pseudomonas putida*

by

Alberto Sánchez-Pascuala[a1], Lorena Fernández-Cabezón[b],
Víctor de Lorenzo[a]*, and Pablo I. Nikel[b]*

[a] Systems and Synthetic Biology Program, Centro Nacional de Biotecnología (CNB-CSIC), Campus de Cantoblanco, 28049 Madrid, Spain

[b] The Novo Nordisk Foundation Center for Biosustainability, Technical University of Denmark, 2800 Kongens Lyngby, Denmark

[1] **Current address:** The Max Planck Institute for Terrestrial Microbiology; Karl-von-Frisch-Straße 10, 35043 Marburg, Germany

Keywords: *Pseudomonas putida*, glycolysis, metabolic engineering, glucose, synthetic metabolism, synthetic biology

Running title: Engineering linear glycolysis in *Pseudomonas putida*

* Correspondence to: *Víctor de Lorenzo* (vdlorenzo@cnb.csic.es)
Centro Nacional de Biotecnología (CNB-CSIC)
Madrid, Spain
Tel: (+34 91) 585 45 73

Pablo I. Nikel (pabnik@biosustain.dtu.dk)
The Novo Nordisk Foundation Center for Biosustainability,
Technical University of Denmark
Lyngby, Denmark
Tel: (+45 93) 51 19 18

ABSTRACT

The core metabolism for glucose assimilation of the soil bacterium and platform strain *Pseudomonas putida* KT2440 has been reshaped from the native, cyclically-operating Entner-Doudoroff (ED) pathway to a linear Embden-Meyerhof-Parnas (EMP) glycolysis. The genetic strategy deployed to obtain a suitable host for the synthetic EMP route involved not only eliminating enzymatic activities of the ED pathway, but also erasing peripheral reactions for glucose oxidation that divert carbon skeletons into the formation of organic acids in the periplasm. Heterologous glycolytic enzymes, recruited from *Escherichia coli*, were genetically knocked-in in the mutant strain to fill the metabolic gaps for the complete metabolism of glucose to pyruvate through a synthetic EMP route. A suite of genetic, physiological, and biochemical tests in the thereby-refactored *P. putida* strain—which grew on glucose as the sole carbon and energy source—demonstrated the functional replacement of the native sugar metabolism by a synthetic catabolism. ^{13}C-labelling experiments indicated that the bulk of pyruvate in the resulting strain was generated through the metabolic device grafted in *P. putida*. Strains carrying the synthetic glycolysis were further engineered for carotenoid synthesis from glucose, indicating that the implanted EMP route enabled higher carotenoid content on biomass and yield on sugar as compared with strains running the native hexose catabolism. Taken together, our results highlight how conserved metabolic features in a platform bacterium can be rationally reshaped for enhancing physiological traits of interest.

1. Introduction

Because of its naturally-evolved metabolic and stress-tolerant qualities, *Pseudomonas putida* KT2440 constitutes a prime example of an environmental bacterium that has been established as an attractive host for biotechnological applications (Belda et al., 2016; Calero and Nikel, 2019; Nelson et al., 2002; Nikel and de Lorenzo, 2018). Among other reasons, this occurrence stems from the architecture of its central carbon metabolism, which has evolved to ensure survival in the natural environments where this species is usually found—often characterized by changing and extreme physicochemical conditions (Ebert et al., 2011; Martins dos Santos et al., 2004). Glucose catabolism in *P. putida* KT2440 relies on the Entner-Doudoroff (ED) pathway (Chavarría et al., 2012; del Castillo et al., 2007; Fuhrer et al., 2005), which processes 6-phosphogluconate (6PG) formed *via* separate (and converging) routes for sugar phosphorylation (trunk) or oxidation (peripheral) (Sudarsan et al., 2014). A fraction of the triose pool generated thereof is recycled back to hexoses-*P* by a particular metabolic architecture, termed *EDEMP cycle*, which involves a combination of activities from the ED, an incomplete Embden-Meyerhof-Parnas (EMP), and pentose phosphate (PP) pathways (Kohlstedt and Wittmann, 2019; Nikel et al., 2015). This particular biochemical wiring enables *P. putida* to boost catabolic production of NADPH—at the expense of ATP and NADH generation. As such, the EDEMP cycle in *P. putida* KT2440 is a relevant example of metabolic adaptation evolved to counteract adverse environmental conditions (Nikel and Chavarría, 2016). Apart from catabolic NADPH overproduction, such cyclic operation of central glycolytic pathways allows for a broader interconnectivity of key metabolic intermediates—a relevant feature for bacteria, like *Pseudomonas* species, which can grow on a variety of structurally unrelated carbon substrates (Chavarría et al., 2016; del Castillo et al., 2008; Jiménez et al., 2002; Lessie and Phibbs, 1984), some of which are known to constitute a source of stress (Benedetti et al., 2016; Blank et al., 2008; de Lorenzo and Loza-Tavera, 2011; Poblete-Castro et al., 2019). On the other hand, the operation of the EDEMP cycle yields half the amount of ATP per sugar molecule as compared to the linear EMP pathway (**Fig. 1a**) (Flamholz et al., 2013; Peekhaus and Conway, 1998). This situation suggests that the metabolism of *P. putida* favors stress resistance in detriment of biomass formation, a feature undoubtedly useful to survive in harsh environmental niches (Chavarría et al., 2013; Dvořák et al., 2017).

The absence of a functional EMP pathway in strain KT2440 can be traced to the lack of the key glycolytic 6-phosphofructo-1-kinase (Pfk) activity. However, the addition of the PfkA enzyme from *Escherichia coli* K-12 into the biochemical network of *P. putida* did not suffice to activate an EMP route for glucose consumption (Chavarría et al., 2013), even when the ED pathway was genetically blocked. The *GlucoBrick* platform, a set of standard glycolytic modules encoding all the EMP enzymes from *E. coli* K-12 in a fixed format, has been thus designed as a tool for engineering glycolysis in Gram-negative bacteria (Sánchez-Pascuala et al., 2017; 2018). The GlucoBrick platform is composed by two modules, each of them consisting of five individual *bricks*. Module I (GBI) encodes the enzymes of the *preparatory phase*, which uses ATP to convert hexoses into trioses-*P* [i.e. glucose → glyceraldehyde-3-*P* (GA3P)] (**Fig. 1b**). Module II (GBII) encodes the enzymes of the *pay-off phase*, the second half of the EMP route, and it converts trioses phosphate into pyruvate (Pyr) (i.e. GA3P → Pyr). With these portable metabolic modules in hand—and the panoply of genetic tools available for editing the genome of *P. putida* (Martínez-García and de Lorenzo, 2017; Wirth et al., 2019)—the present work explores the deep metabolic refactorization of strain KT2440, in which the ED pathway (and the EDEMP cycle thereof) is replaced by a rationally-designed, synthetic EMP glycolysis. Our results demonstrate that the careful rewiring of native biochemical pathways and the genetic grafting of an artificial glycolysis device enables glucose-dependent growth of *P. putida via* a linear pathway for sugar catabolism. These developments not only open new possibilities of bacterial *chassis* engineering for creating novel whole-cell biocatalysts, but also rise interesting questions on how the core metabolism defines species identity.

2. Materials and Methods

2.1. Bacterial strains, plasmids, and culture conditions

The bacterial strains employed in this study are listed in **Table 1**. *E. coli* and *P. putida* cultures were incubated at 37ºC and 30ºC, respectively. For propagation and construction of plasmids, *E. coli* strains CC118 and DH5α λ*pir* were grown in lysogeny broth (LB) medium (Green and Sambrook, 2012; Martínez-García et al., 2017). For physiology experiments, and to obtain cell-free extracts to be used in enzyme activity assays, bacterial cells were grown with rotatory

shaking at 170 r.p.m. in 250-ml Erlenmeyer flasks filled with 50 ml of M9 minimal medium, containing 6 g l^{-1} Na_2HPO_4, 3 g l^{-1} KH_2PO_4, 1.4 g l^{-1} $(NH_4)_2SO_4$, 0.5 g l^{-1} NaCl, and 0.2 g l^{-1} $MgSO_4 \cdot 7H_2O$ (Nikel and de Lorenzo, 2013b). Unless otherwise indicated, minimal medium cultures were added with glucose at 20 mM or succinate at 30 mM. The same concentration of carbon atoms (120 mM) was adopted when cultures were inoculated under either glycolytic (glucose) or gluconeogenic (succinate) conditions. In order to adapt the cells to grow on glucose from rich LB medium, pre-inocula were prepared with a few isolated colonies picked from LB medium plates. Pre-inocula were grown overnight (ca. 12 h, with the exception of engineered strains with a low growth rate, which were grown for 24-36 h) in 20 ml of M9 glucose minimal medium with the corresponding antibiotics in 100-ml Erlenmeyer flasks, and these cultures were used to seed working cultures to an optical density measured at 600 nm (OD_{600}) of ca. 0.05. Normalized growth coefficients were calculated according to Nikel et al. (2013). In the case of solid culture media, the composition was the same of the corresponding liquid media with the addition of 15 g l^{-1} of agar. The antibiotics employed for selection were added whenever needed at the following final concentrations: ampicillin (Ap), 150 μg ml^{-1} for *E. coli* strains or 500 μg ml^{-1} for *P. putida* strains; gentamicin (Gm), 10 μg ml^{-1}; and kanamycin (Km), 50 μg ml^{-1}. In some cultures, isopropyl-1-thio-β-galactopyranoside (IPTG) was added at 1 mM to induce the $LacI^Q/P_{trc}$ expression system. During the construction of *P. putida* mutants, sodium 3-methylbenzonate (3-*m*Bz) was used at 15 mM to induce the XylS-dependent *Pm* promoter, driving the expression of the gene encoding the I-*Sce*I homing nuclease. The same inducer (3-*m*Bz) was used at 0.5 mM to trigger the XylS/*Pm*-dependent expression of the *crt* genes in carotenoid synthesis experiments. For long-term preservation, bacteria were frozen in LB medium containing 20% (v/v) glycerol and kept at –80ºC.

2.2. DNA manipulation and sequencing, construction of mutant strains and assembly of a synthetic pathway for carotenoid synthesis, and bacterial transformation

The plasmids and oligonucleotides used in this study are listed in **Table S1** and **S2**, respectively, in the Supplementary Material. DNA manipulations were carried out following routine laboratory techniques (Green and Sambrook, 2012). Plasmid DNA purification was done with the QIAprep Spin Miniprep kit (Qiagen Inc., Valencia, CA, USA) according to the manufacturer's instructions.

Restriction and DNA modification enzymes were purchased from New England BioLabs (Ipswich, MA, USA). Synthetic oligonucleotides were ordered from Sigma-Aldrich (St. Louis, MO, USA). Isolate colonies from fresh LB plates were used as the starting material for colony polymerase chain reaction (PCR) amplifications to check for the presence of plasmids or gene deletions. PCR products were purified with the NucleoSpin Extract II kit (Macherey-Nagel, Düren, Germany). Agarose gel visualization was possible with the use of VersaDoc™ apparatus (Bio-Rad Corp., Hercules, CA, USA). DNA sequencing (Secugen, Madrid, Spain) was used to check the accuracy of all constructs. Clean *P. putida* mutants were obtained following the protocol described by Martínez-García and de Lorenzo (2011); the detailed protocol for the construction of mutants is described in the Supplementary Material. Plasmid pPS1·CRT, carrying the *crtEBIY* genes from the Gram-negative Enterobacterium *Pantoea ananatis* (**Table S1** in the Supplementary Material), was constructed for carotenoid synthesis. The expression plasmid was assembled by means of *USER* cloning (Nour-Eldin et al., 2010). Individual DNA fragments were amplified by PCR using *Phusion U* Hot Start DNA Polymerase (Thermo Scientific, Waltham, MA, USA), which can extend DNA fragments containing uracil residues. Vector pPS1 (Calero et al., 2016) was reverse-amplified as the backbone by using primers pPS1*crtEBIY*-UC-F and pPS1*crtEBIY*-UC-R, forming single-stranded DNA overhangs compatible with primers *crtEBIY*-UC-F and *crtEBIY*-UC-R—separately used to amplify the *crtEBIY* gene cluster from plasmid pSEVA13-sl3T7-*crtEBIY* (Kim et al., 2016) as the template. The resulting pPS1·CRT plasmid carries the *crtEBIY* gene cluster from *P. ananatis* under transcriptional control of a XylS/*Pm* regulatory element.

Transformation of *E. coli* strains was carried out either (i) chemically, with the $RbCl_2$ method to obtain competent cells (Green and Sambrook, 2012), or (ii) by electroporation as described by Datsenko and Wanner (2000). In the case of *P. putida* transformations, electrocompetent cells were obtained by washing the biomass with 300 mM sucrose at room temperature (Choi et al., 2006). All electroporations were performed in a Gene Pulser/Pulse Controller (Bio-Rad Corp.) system configured at 2.5 kV, 25 μF, and 200 Ω.

2.3. In silico prediction of gene function and use of online databases

The function of some genes, for which no experimental data was available, has been explored *in silico* using curated genome databases. The web resources used in this study were the MicroScope platform available at http://www.genoscope.cns.fr/agc/microscope (Vallenet et al., 2017) and the *Pseudomonas* Genome Database available at http://www.pseudomonas.com (Winsor et al., 2016).

2.4. Preparation of cell-free extracts and in vitro enzymatic assays

Cell-free extracts of *E. coli* and *P. putida* were obtained by a modification of published protocols (Chavarría et al., 2016; Corona et al., 2018; Nikel et al., 2014a; Ruiz et al., 2006). A detailed description of the procedures and the specific methods used for *in vitro assays* of Edd, Gad, Gcd, Glk, and Pfk can be found in the Supplementary Material. The limit of detection for all the enzymatic assays described in this study was below 2 nmol min^{-1} mg $protein^{-1}$.

2.5. Other analytical determinations

Experiments requiring quantification of residual glucose in culture supernatants were performed by adapting a protocol based on the glucose assay kit (Sigma-Aldrich Co.) into 96-well microtiter plates (Nunclon™Δ Surface; Nunc A/S, Roskilde, Denmark). The assay reagent was prepared as indicated in the technical bulletin; the final mix per well contained 80 μl of the assay reagent, 40 μl of the sample (diluted with water to yield approximately 20-80 μg glucose ml^{-1}), and 80 μl of 12 N H_2SO_4. The amount of the final pink-colored product (oxidized *o*-dianisidine) was quantified at 540 nm using a SpectraMax™ M2e multi-mode microplate reader (Molecular Devices LLC, Sunnyvale, CA, USA). The supernatants for these determinations were obtained by centrifugation of 50-ml cultures harvested in mid-exponential phase (i.e. corresponding to an OD_{600} of ca. 0.5) at 4000 r.p.m. for 15 min at 4°C.

2.6. Quantification of intracellular metabolite concentrations

P. putida cultures (the wild-type strain carrying the empty vector pSEVA224, and the GC1 mutant harboring plasmid pS224·GBI) were grown in M9 minimal medium added with glucose at 20 mM, 50 μg ml^{-1} Km, and 1 mM IPTG. When the cultures reached the mid-exponential phase (i.e. OD_{600} of *ca*. 0.5), the biomass corresponding to 0.5-0.6 mg of cell dry weight (CDW) was collected in duplicates by fast centrifugation (13,000 r.p.m., 30 s, –4ºC). Bacterial pellets were immediately frozen by immersing the cell sediment in liquid N_2. Samples were then extracted three times with 0.5 ml of 60% (v/v) ethanol buffered with 10 mM ammonium acetate (pH = 7.2) at 78°C for 1 min. After each extraction step, the biomass was separated by centrifugation at 13,000 r.p.m. for 1 min. The three liquid extracts were pooled in a new tube and dried at 120 μbar, and finally stored at –80°C. Samples were re-suspended in 20 μl of MilliQ water and injected into a Waters Acquity UPLC system (Waters Corp., Milford, MA, USA) with a Waters Acquity T3 column (150 mm × 2.1 mm × 1.8 μm, Waters Corp.) coupled to a Thermo TSQ Quantum Ultra triple quadrupole instrument (Thermo Fisher Scientific Inc., Waltham, MA, USA) with electrospray ionization. The quantitative analysis of raw metabolomic data and the normalization procedure were conducted as explained by van der Werf et al. (2008) and Nikel et al. (2015). Carotenoids were analytically quantified by extracting the biomass upon harvesting cells from 24-h glucose cultures in M9 minimal medium (added with glucose, Km, Gm, IPTG, and 3-*m*Bz). Cell material, corresponding to an OD_{600} = 3, was harvested by centrifugation (13,000 r.p.m., 5 min, 4ºC). Cells were resuspended in 50 μl of water before extraction with 1 ml of acetone, and all the operations were carried out in the dark. The bacterial biomass was extracted with the solvent three times; the extracts were pooled and dried under a gentle N_2 current. Dried extracts were kept at –80°C until analysis, when the sediment was resuspended in 20 μl of ethanol just prior to analysis. Pigment extracts were centrifuged again as indicated above, and the absorption was immediately determined spectrophotometrically at 450 nm. Total carotenoid concentrations were assessed in these samples using a molar extinction coefficients for β,β-carotene of ε = 140,500 M^{-1} cm^{-1} (Britton et al., 2004). Ethanolic extracts were also subjected to gas chromatography coupled to mass spectrometry (GC-MS) analysis for precise carotenoid quantification as indicated by Stutz et al. (2015).

2.7. Analysis of the contribution of the synthetic glycolysis to pyruvate biosynthesis by positional enrichment using ^{13}C-labelled substrates

The relative contribution of the EMP, ED, and PP pathways to glucose catabolism (at the level of the Pyr node) was assessed by analyzing the ^{13}C-labeling pattern of proteinogenic alanine (Ala), generated during growth on [1-$^{13}C_1$]-glucose. To this end, the bacterial strains under study were grown as indicated in *Sections 2.1* and *2.6*, but using [1-$^{13}C_1$]-glucose (Cambridge Isotope Laboratories, Tewksbury, MA, USA) at 20 mM as the carbon source. Inocula for these working cultures were likewise prepared in the presence of 20 mM [1-$^{13}C_1$]-glucose. Cells were collected from 10-ml culture aliquots by centrifugation (10,000 r.p.m., 5 min, 4ºC) when the cultures reached OD_{600} = 0.5, and pellets were rapidly washed twice with deionized water. Prior to GC-MS analysis, the cellular protein was hydrolyzed for 24 h at 105°C using 50 μl of 6 M HCl per mg of CDW (Nikel et al., 2015). Cell debris was removed by filtration (Ultrafree-MC centrifugal filter; Millipore, Billerica, MA, USA). The labeling patterns of proteinogenic Ala were analyzed using its *tert*-butyldimethylsilyl derivative (Nanchen et al., 2007) in an Agilent 7890A GC-MS equipped with a 5975C quadrupole mass selective detector (Agilent Technologies, Waldbronn, Germany). The relative fraction of the non-labeled mass isotopomers (M_0) of the entire Ala molecule with carbon atoms C_1, C_2, and C_3 (Ala^{123}) and of a fragment that contained the two carbon atoms C_2 and C_3 (Ala^{23}) were assessed to determine the origin of Pyr essentially as explained by Klingner et al. (2015). Individual labeled fractions were obtained from mass analysis of *tert*-butyldimethylsilyl—derivatized Ala at a mass-to-charge (*m*/z) ratio for the monoisotopic mass of 260 (Ala^{123}) and 232 (Ala^{23}). Natural isotope abundances in the samples were corrected as explained by Nikel et al. (2009). Anaplerotic fluxes were accounted for by the amount of oxaloacetate derived from Pyr, and phosphoenolpyruvate derived from oxaloacetate (Chavarría et al., 2012). The relative fluxes into the ED pathway (f_{ED}), the EMP pathway (f_{EMP}), and the PP pathway (f_{PP}) were derived from these measurements as $f_{ED} = 1 - f_{PP} - f_{EMP}$, $f_{EMP} = -2\times(M_0,Ala^{23} - 1)$, and $f_{PP} = 2\times(M_0,Ala^{123} - 0.5)$, respectively. The calculation of the respective fluxes *via* the labeling pattern of proteinogenic serine (Fürch et al., 2009) yielded the same results.

2.8. Data and statistical analysis

All the experiments reported were independently repeated at least twice (as indicated in the corresponding figure or table legend), and the mean value of the corresponding parameter ± standard deviation is presented. In some cases, the level of significance of the differences when comparing results was evaluated by means of the Student's *t* test with α = 0.01 or α = 0.05 as indicated in the figure legends.

3. Results and Discussion

3.1. Metabolic debugging of branched pathways for glucose in P. putida KT2440

We started by inspecting the biochemical reactions in central carbon metabolism of *P. putida* KT2440 (**Fig. 2**) that should be eliminated for constructing a glycolytic *chassis* (GC) that could host an artificially-assembled EMP glycolytic route. Core (trunk) and peripheral pathways for sugar processing were targeted for substrate channeling into the intended synthetic route. Glucose can be processed in two different ways in *P. putida* KT2440: (i) direct phosphorylation in the cytoplasm *via* the glucokinase activity (Glk) encoded by the *glk* gene (*PP_1011*), and (ii) oxidation in the periplasmic space *via* the glucose dehydrogenase activity (Gcd) encoded by the *gcd* gene (*PP_1444*) and the gluconate 2-dehydrogenase activity (Gad), the genetic source of which is yet to be defined. We thus set to eliminate the genes encoding all three enzymatic activities in strain KT2440 and to identify, at the same time, the genetic determinants of the Gad activity in this bacterium.

The first issue to solve was the branching generated by the Glk and Gcd activities. The *glk* gene encodes the main (and probably only) hexose kinase activity in *P. putida* KT2440 (del Castillo et al., 2007). Glk converts glucose into glucose-6-*P* (G6P) in the cytoplasm (**Fig. 2**), and this metabolic intermediate can be transformed into 6PG by the sequential action of Zwf (G6P dehydrogenase, represented by three isozymes in strain KT2440) and Pgl (6-phosphogluconolactonase). 6PG stemming from this phosphorylation branch represents ca. 10% of the glucose entering the core biochemical network (Nikel et al., 2015), which indicates that the

peripheral oxidation loop for sugars is preferred in this bacterial species. The Gcd activity is executed by the protein encoded by the single *gcd* gene (*PP_1444*) (del Castillo et al., 2007). This enzyme is an example of inner membrane-bound glucose dehydrogenase (An and Moe, 2016), that requires the redox cofactor pyrroloquinoline quinone (PQQ). Gcd allows *P. putida* KT2440 to transform glucose into gluconate in the periplasmic space (**Fig. 2**)—a rather relevant role if one considers that almost 90% of the glucose that enters the central carbon metabolism of this bacterium gets oxidized (Nikel et al., 2015). Transformation of glucose into oxidized products is counterproductive for our engineering purposes, as the use of hexoses in peripheral reactions competes with the intended linear glycolysis.

On this basis, the *glk* and *gcd* genes in strain KT2440 were independently eliminated and the biochemical characterization and growth profile displayed by the parental strain was compared to the Δ*glk* and Δ*gcd* mutants (**Fig. 3**). Deletion of *glk* and *gcd* resulted in the loss of any detectable Glk and Gcd activity, respectively, in the corresponding *P. putida* mutants (**Fig. 3a**). At the same time, individually blocking either the phosphorylative (Δ*glk*) or the oxidative (Δ*gcd*) branches of hexose processing did not result in any evident cross-regulation effects on the other (remaining) activity. In other words, removing the Glk activity from *P. putida* does not result in a different pattern of Gcd activity—and *vice versa*. The glucose-dependent growth of the Δ*gcd* mutant was more affected than that of the Δ*glk* strain (μ = 0.33 h^{-1} *versus* μ = 0.45 h^{-1}, respectively) when bacteria were grown in M9 minimal medium with 20 mM glucose as the sole carbon source (**Fig. 3b**). The growth phenotype of the Δ*gcd* strain did not involve a dramatic effect in terms of overall fitness (as indicated by the extension of the lag phase and final biomass density, which did not differ significantly from the values observed in the parental strain)—but, again, it could reflect the preference of this bacterium to metabolize glucose mainly by the oxidative branch. Additionally, the absence of Glk and Gcd activities were not deemed relevant for growth under gluconeogenic conditions, i.e. in M9 minimal medium with 30 mM succinate (**Fig. 3b**). Interestingly, the growth rates recorded for all the strains under study in microtiter plate cultures were similar, irrespective of the substrate used. As expected, the accumulation of the Δ*glk* and Δ*gcd* deletions in the same strain prevented the resulting mutant from growing on glucose as the sole carbon source. This observation contrasts with the marginal impact that the individual deletions displayed on growth, highlighting the robustness of central carbon metabolism in *P. putida* KT2440.

3.2. Identification of genes encoding 2-gluconate dehydrogenase (Gad) in P. putida KT2440 and construction of a strain devoid of Gad activity

Even when blocking the Gcd step of the peripheral oxidation loop was enough to prevent the utilization of glucose *via* the oxidative branch, we explored the genetic determinants of the Gad activity in strain KT2440 to avoid potential misrouting of metabolic intermediates or unexpected interactions due to the presence of latent oxidative activities (Miller and Raines, 2004). Based on the *in silico* analysis of the genome of *P. putida* KT2440, the Gad activity is presumed to be catalyzed by an enzymatic complex comprising three different gene products: PP_3382, PP_3383, and PP_3384 (**Fig. 4a**). The Gad activity is driven by a membrane-bound flavin adenine dinucleotide (FAD)-containing gluconate 2-dehydrogenase (FAD-GADH) (McIntire et al., 1985). Such FAD-GADH activity has been characterized to some extent in *P. aeruginosa* (Hunt and Phibbs, 1983; Matsushita et al., 1982), allowing us to identify the orthologues in *P. putida* KT2440. Analysis of the corresponding genomic regions revealed the following features: (i) the largest subunit of the complex is encoded by *PP_3383* (with a product of 594 amino acids) and comprises the dehydrogenase subunit that contains FAD as the prosthetic group, covalently bound to the histidine residue of the polypeptide (McIntire et al., 1985); (ii) the middle subunit (with a product of 417 amino acids) is encoded by *PP_3382* and contains the heme *c* cofactor, which probably facilitates the electron transfer from the FAD moiety in the dehydrogenase to the ubiquinone carrier in the inner membrane, thus connecting sugar oxidation with the respiratory chain (Matsushita et al., 1994); and (iii) the small subunit (with a product of 246 amino acids) is encoded by *PP_3384* and it was recently annotated *in silico* as a γ subunit of the FAD-GADH complex (Belda et al., 2016).

Despite the fact that the literature offers examples of biotechnological applications based on the use of the PP_3382-4 enzymatic complex (Yu et al., 2018), the function of Gad has not been yet proved *via* generation of mutant *P. putida* strains. In this work, the complete, in-frame removal of the group of genes *PP_3382-4* was achieved by a single deletion event. The gene pair *PP_3382* and *PP_3383* has a properly annotated function both in the *Pseudomonas* database (Winsor et al., 2016) and in the resequencing of the genome of strain KT2440 (Belda et al., 2016). As indicated above, *PP_3384* has been annotated *in silico* as γ subunit of the FAD-GADH complex,

and it was removed taking into account studies in other bacterial species, indicating a key role of FAD-GADH in sugar oxidation (Arellano et al., 2010). Additionally, the relevance of the products encoded by *PP_3623* and *PP_4232* in the overall Gad activity was evaluated by eliminating the corresponding coding sequences. The *in silico* annotation identifies *PP_3623* (encoding a product of 447 amino acids), as the cytochrome *c* subunit of an alcohol dehydrogenase. At the same time, *PP_3623* is considered to be a duplication of *PP_3382* with a high level of statistical significance. *PP_4232* (encoding a product of 403 amino acids) has not been assigned any function but is also considered to be a *PP_3382* duplication. Taking into account this information, the deletion of both *PP_3623* and *PP_4232* was implemented along the elimination of *PP_3382-PP_3384* in order to completely remove the Gad activity in *P. putida* KT2440 (**Fig. 4a**)—shedding light, at the same time, on the existing knowledge about oxidative carbon metabolism in strain KT2440.

According to the results of **Fig. 4b**, the pool of genes involved in the oxidation of gluconate into 2-ketogluconate could be unambiguously identified. The bulk Gad activity could be traced to the products encoded by the *PP3382-4* operon; the polypeptides encoded by *PP_3623* and *PP_4232* displaying a marginal influence in the Gad activity. On the other hand, the removal of the Gad activity resulted largely irrelevant in terms of bacterial fitness, since very similar specific growth rates were observed in all the *P. putida* mutants and the parental strain when evaluated under glycolytic (M9 minimal medium with 20 mM glucose) or gluconeogenic (M9 minimal medium with 30 mM succinate) growth conditions (**Fig. 4c**). Once the peripheral pathways of sugar utilization had been eliminated, we set out to block the default catabolic route for G6P as explained below.

3.3. Elimination of the Entner-Doudoroff pathway in P. putida KT2440 and physiological characterization of mutant strains

Given the lack of Pfk in *P. putida* (Latrach-Tlemçani et al., 2008; Vicente and Cánovas, 1973a, b), the only way that glucose can be metabolized in this species is through the ED pathway. This route enables *P. putida* KT2440 to obtain Pyr and GA3P from glucose—key intermediates for hexoses-*P* regeneration through the EDEMP cycle—and to obtain energy and reducing power by means of the tricarboxylic acid cycle (Nikel et al., 2016; 2015). The ED pathway is composed by the sequential activity of Edd, encoded by the *edd* gene (*PP_1010*), which transforms 6PG into 2-

keto-3-deoxy-6-phosphogluconate (KDPG); and Eda, encoded by the *eda* gene (*PP_1024*), which transforms KDPG into Pyr and GA3P (Nikel et al., 2014b). The next stage in the stepwise construction of *P. putida* GC was to remove the first component of ED catabolism (i.e. the Edd activity). Under this scenario, *P. putida* would be unable to grow on glucose as a sole carbon source—and its glucose-dependent growth phenotype can only be rescued by the functional implementation of a linear glycolysis. **Fig. 5** summarizes the growth phenotypes of the in-frame *P. putida* mutants constructed thus far under both glycolytic and gluconeogenic growth conditions. Moreover, the normalized growth coefficients calculated from growth parameters in liquid cultures indicate that (i) the Δ*gcd* mutant is the only strain slightly affected when growing on glucose as the sole carbon source, and (ii) the Δ*gcd* Δ*glk* double mutant and the Δ*edd* mutant are unable to grow on glucose, and are affected even under gluconeogenic growth conditions. With all this information at hand, the next step was to purposefully combine the individual deletions in metabolic genes and implant a linear glycolysis in *P. putida* as disclosed below.

3.4. Construction of a glycolytic chassis and metabolic grafting of a synthetic EMP device into P. putida KT2440

Our previous efforts in activating an EMP pathway in *P. putida* indicated that the mere knock-in of a Pfk activity into the native biochemical network is not only insufficient to enable a linear glycolysis, but also detrimental for the overall cell physiology (Chavarría et al., 2013). Against this background, our current engineering approach included (i) multiple knock-out of genes encoding both central and peripheral routes for sugar metabolism in *P. putida* and (ii) controlled expression [by means of an IPTG-inducible $LacI^{Q}/P_{trc}$ regulatory element; Silva-Rocha et al. (2013)] of a standardized gene cluster encoding the five enzymes of the preparatory phase of the EMP pathway. A strain was thereby constructed by accumulation of the in-frame Δ*glk*, Δ*gcd*, Δ*gad* (i.e. Δ*PP_3382-4*, Δ*PP_3623*, and Δ*PP_4232*), and Δ*edd* mutations in *P. putida* KT2440, resulting in *P. putida* GC1 (**Table 1**). Upon introduction of Module I of the GlucoBrick platform (Sánchez-Pascuala et al., 2017; 2018) in the *P. putida* GC1 strain, the expected carbon flow would connect G6P with Pyr *via* the designed EMP pathway (**Fig. 6a**). Note that we decided to implement the *whole* Module I of the linear glycolysis of *E. coli* (although some enzymes of the pathway are

native to *P. putida* GC1) to ensure improved metabolic channeling and reducing the risk of potential bottlenecks in the biochemical network (Hollinshead et al., 2016).

A simple growth experiment was first carried out by streaking the bacterial strains under study onto M9 minimal medium plates containing either glucose or succinate and the appropriate additives (**Fig. 6b**). Both the wild-type strain and *P. putida* GC1 were transformed either with the empty, low-copy-number pSEVA224 vector or the plasmid expressing Module I from the GlucoBrick platform (pS224·GBI), and plates were incubated for 36 h at 30°C. Expectedly, both strains grew well under gluconeogenic conditions (i.e. using succinate), and *P. putida* GC1 carrying pSEVA224 could not grow on glucose as the sole carbon source. In contrast, *P. putida* GC1 transformed with plasmid pS224·GBI was able to grow on glucose in a similar fashion as observed in succinate-containing plates. In other words, the enzyme activities encoded in Module I allowed *P. putida* GC1 to metabolize glucose *via* the synthetic EMP pathway. Since all the strains grew on succinate as the sole carbon source, the genetic manipulations of strain GC1 do not seem to significantly affect bacterial growth *via* gluconeogenesis. Further characterization of the strains at stake in liquid cultures confirmed the growth phenotypes observed in solid media (**Fig. 6c**). In glucose cultures, the specific growth rate of *P. putida* GC1 transformed with plasmid pS224·GBI was ca. 10% of that in the wild-type strain containing the empty vector. This impaired growth is somewhat expected due to the large number of modifications introduced in strain GC1—including several mutations in native components of central carbon metabolism, which are likely preferred over exogenous routes. Oxygen limitation could also play a role, considering that *P. putida* is an obligate aerobe (Nikel and de Lorenzo, 2013b). In addition to the decrease in the specific growth rate, the final cell density was also affected in cultures of *P. putida* GC1 transformed with plasmid pS224·GBI (i.e. a 35% reduction in the final OD_{600} values as compared to that of *P. putida* KT2440 transformed with pSEVA224). In any case, the glucose-dependent growth phenotype served as a proof-of-concept that the designed glycolytic device was functional in the rewired *P. putida* strain. Yet, what are the levels of the key enzymatic activities in this engineered strain?

3.5. Biochemical and metabolomic characterization of the glycolytic device implanted in P. putida KT2440

Once the possibility of implementing a functional linear EMP pathway in *P. putida* GC1 as the sole glycolytic route was demonstrated, the observed glucose-dependent growth phenotype was correlated with the presence of enzymes encoded by the GlucoBrick genes. To this end, the Glk and Pfk activities (the first enzyme of the synthetic glycolytic device and the enzyme missing in strain KT2440, respectively) were determined in cell-free extracts of the relevant strains grown in M9 minimal medium containing glucose (**Fig. 7**). The native Glk activity could be detected in *P. putida* KT2440 and in wild-type *E. coli* BW25113 (used here as a control strain) carrying the empty vector (i.e. pSEVA224), upon induction of gene expression with IPTG. The Glk activity in strain KT2440 was almost twice that of *E. coli* (**Fig. 7a**). The same activity was determined in *P. putida* KT2440 Δ*glk* and in *E. coli* BW25113 Δ*glk* Δ*ptsI* (i.e. an *E. coli* strain completely deficient in glucose phosphorylation), carrying the empty pSEVA224 vector and added with IPTG. Predictably, no significant Glk activity was detected in either mutant. Finally, hexose phosphorylation was tested in *P. putida* GC1 containing plasmid pS224·GBI. The only possible way for this bacterium to grow on glucose is linked to the presence of the Glk activity encoded by Module I of the GlucoBrick platform. Indeed, *P. putida* GC1 carrying plasmid pS224·GBI (and induced with IPTG) had a specific Glk activity 130-fold higher than that of the wild-type strain carrying the empty plasmid (**Fig. 7a**). This high level of enzyme activity can result from unregulated expression of the *glk* gene, alongside to the extra gene copies in the cells due to the expression of Module I in a plasmid format—and also from a potentially different pattern of enzyme regulation of Glk from *E. coli* in a heterologous context (Heredia et al., 2006).

The specific Pfk activity was likewise assessed in *E. coli* BW255113 and its Δ*pfkA* Δ*pfkB* double mutant derivative (termed Δ*pfk* in **Fig. 7b**) carrying the empty pSEVA224 vector in IPTG-induced glucose cultures. The Pfk activity was determined in these two *E. coli* strains as a positive and negative control of F6P phosphorylation, respectively, considering that *P. putida* KT2440 lacks the Pfk-dependent conversion of F6P into FBP (**Fig. 2**). As expected, the Pfk activity tested positive in the wild-type *E. coli* strain, in contrast to the very low level of activity detected in *E. coli* Δ*pfk* and in *P. putida* KT2440 carrying the empty pSEVA224 vector (**Fig. 7b**). It was assumed

that the Pfk activity must be present in *P. putida* GC1 carrying plasmid pS224·GBI, as this would be the only way to bestow growth on glucose. The *in vitro* biochemical determinations support this notion, as the engineered strain had a 32-fold increase in the Pfk activity compared with wild-type *E. coli* BW255113 (**Fig. 7b**). Similarly to Glk, the high level of Pfk activity detected in *P. putida* GC1 carrying plasmid pS224·GBI can result from unregulated expression of the *pfkA* gene [taking into account that this activity is alien to the host; Alves et al. (1997)], alongside to the extra gene copies in the cells due to the expression of Module I in a plasmid format.

The implementation of Module I in *P. putida* GC1 is also expected to result in differences in terms of glucose utilization. The glucose consumption was evaluated during exponential growth of both wild-type *P. putida* KT2440 and *P. putida* GC1 carrying either an empty pSEVA224 vector or plasmid pS224·GBI, respectively (**Fig. 7c**). Glucose consumption increased by ca. 2-fold in *P. putida* GC1 bearing plasmid pS224·GBI as compared with the strain KT2440 transformed with the empty pSEVA224 vector. This physiological feature mirrors the increased activity of the enzymes borne by the GlucoBrick platform in *P. putida* GC1 (**Fig. 7a** and **b**). As the pattern of enzymatic activities and sugar consumption was remarkably different in the engineered strain, we also explored its metabolomic fingerprint under the same growth conditions (**Table 2**). To this end, the intracellular content of the key glycolytic intermediates G6P, fructose-6-*P*, dihydroxyacetone-*P*, and Pyr were determined both in the parental strain carrying the empty pSEVA224 vector and *P. putida* GC1 transformed with plasmid pS224·GBI by liquid chromatography coupled to mass spectrometry. All metabolic intermediates had increased levels in the engineered strain expressing the glycolytic device; GA3P and Pyr, for instance, had a 2.2- and 2.8-fold higher intracellular concentration in *P. putida* GC1 transformed with plasmid pS224·GBI than in the parental strain bearing an empty vector. These trioses serve as a proxy of the entire glycolytic module, as they are the end-products of hexose catabolism afforded by Module I. The results thus far indicate that the increase in glucose consumption in the engineered *P. putida* strain was accompanied by high levels of glycolytic intermediates. The next relevant issue is to solve the metabolic origin of Pyr by feeding the engineered strain with isotopically-labelled substrates as explained in the next section.

3.6. ^{13}C-Labelling experiments identify synthetic glycolysis as the main source of pyruvate in engineered P. putida strains

When cells are fed with a substrate carrying a positional label such as ^{13}C, the isotopic label is passed onto metabolites derived thereof. The resulting labelling pattern can be used to determine the relative activities of different metabolic pathways—and thus the metabolic origin of different intermediates in the biochemical network (Buescher et al., 2015; Fuhrer et al., 2005; Fürch et al., 2009; Klingner et al., 2015). We focused our analysis on the pattern of Pyr labelling, which can be deduced from that of proteinogenic Ala since the carbon backbone of intermediates in central carbon metabolism is preserved in amino acids—an additional advantage of this approach being that proteinogenic amino acids are present in much larger quantities than the metabolic intermediates from which they are synthesized, making the detection easier (Szyperski, 1995). In particular, if the first carbon position of glucose (C1) is uniformly labelled with ^{13}C, i.e. [1-$^{13}C_1$]-glucose, G6P will retain the same positional labelling, and Pyr molecules generated in the ED, EMP, and PP pathways will be isotopically tagged in different ways (**Fig. 8a**). If [1-$^{13}C_1$]-G6P enters the ED pathway, half of the Pyr molecules contains ^{13}C in the C1 position, while the other half is unlabeled. When [1-$^{13}C_1$]-G6P is channeled through the EMP route, half of the resulting Pyr is labelled with ^{13}C in the C3 position, while the remaining half is unlabeled. Finally, the PP pathway will yield unlabeled Pyr as the ^{13}C label is lost to CO_2 *via* GntZ (6PG dehydrogenase, PP_4043). Additionally, Pyr can be generated *via* a set of anaplerotic reactions, which have been shown to be active in strain KT2440 through the Pyr shunt (Chavarría et al., 2012).

Both the wild-type strain transformed with the empty pSEVA224 vector and *P. putida* GC1 bearing plasmid pS224·GBI were grown in M9 minimal medium containing [1-$^{13}C_1$]-glucose as the sole carbon source; the biomass was harvested during mid-exponential growth, and hydrolyzed to assess the labelling pattern of Ala. When the fraction of Pyr molecules coming from different pathways was analyzed in the control strain, the major source of trioses was found to be the ED pathway (**Fig. 8b**). In this case, 95% of Pyr was generated by the activity of the ED route, with a relatively minor contribution from the GA3P → Pyr flux *via* the incomplete EMP pathway and anaplerosis. A negligible involvement of the PP pathway was also evident, in agreement with previous results obtained for wild-type *P. putida* MAD2 (Chavarría et al., 2012). The engineered

P. putida strain expressing the glycolytic module, in contrast, generated 93% of the Pyr molecules through the synthetic EMP pathway. *In vitro* measurements of the Edd activity (the first step in the ED pathway) substantiated this result: *P. putida* GC1 had a very low level of (background) enzyme activity, less than 10% of that in the wild-type strain (**Fig. 8c**). Taken together, these results accredit that (i) the synthetic glycolysis is active in the *P. putida* GC1 background, functionally replacing the native ED route, and (ii) the implanted metabolic module serves as the main source of trioses in the engineered strain—enabling glucose-dependent growth. We then focused on the glucose-dependent synthesis of carotenoids as a proof-of-concept application of the engineered glycolytic strains.

3.7. Enhanced carotenoid synthesis from glucose in engineered P. putida strains

Carotenoids are tetraterpenoids produced by many organisms (Sandmann, 2015) and, from a biotechnological point of view, these C40 hydrocarbons have gained interest for different applications including their use as nutraceuticals or pharmaceuticals (Schweiggert and Carle, 2016; Zhao et al., 2013). In the carotenogenic Gram-negative species *P. ananatis*, the synthesis of carotenoids involves the sequential action of CrtE (geranylgeranyl diphosphate synthase), CrtB (phytoene synthase), CrtI (phytoene desaturase), and CrtY (lycopene cyclase) (Misawa et al., 1990), encoded by the 4.5-kb long *crt* gene cluster (**Fig. 9a**). The key metabolic precursors needed for carotenoid synthesis are Pyr and GA3P, which are firstly transformed by the methylerythritol 4-phosphate (MEP pathway) into the C15 intermediate farnesyl pyrophosphate (**Fig. 9b**). The 4-step carotenoid synthesis pathway finally yields the orange-colored β-carotene product. We reasoned that the introduction of the carotenoid synthesis pathway in engineered *P. putida* strains carrying the synthetic glycolytic module would result in enhanced synthesis of the tetraterpenoid, since the intracellular supply of both Pyr and GA3P trioses is higher than in the wild-type strain (**Table 2**). We constructed plasmid pPS1·CRT for the 3-*m*Bz-inducible, XylS/*Pm*-controlled expression of the *crt* genes from *P. ananatis* (**Table S1** in the Supplementary Material), and transformed both the wild-type strain (carrying the empty pSEVA224 vector) and *P. putida* GC1 (carrying plasmid pS224·GBI) either with plasmid pPS1·CRT or the empty pPS1 vector counterpart. All the engineered strains were aerobically grown in M9 minimal medium containing 20 mM glucose and the appropriate antibiotics and inducers, and the carotenoid content in these

cultures was assessed by GC-MS analysis after 24 h of induction of the expression of the *crt* gene cluster (**Fig. 9c**). Expectedly, we could not detect any carotenoids in acetone extracts obtained from the strains transformed with the empty pPS1 vector. Expression of the *crt* gene cluster from plasmid pPS1·CRT, in contrast, resulted in carotenoid formation both in wild-type KT2440 and *P. putida* GC1 carrying the glycolytic module. The total carotenoid content on biomass was 1.3-fold higher in the strain carrying the synthetic glycolysis than in the wild-type strain, reaching 372 ± 18 μg g_{CDW}^{-1}. These values are in good accordance with a previous report exploring β-carotene biosynthesis in recombinant *P. putida* grown in a rich culture medium (Loeschcke et al., 2013). The yield of carotenoids on glucose was also explored in these cultures as a measure of the efficiency of substrate transformation, and we found that $Y_{carotenoid/glucose}$ was again significantly higher (1.5-fold) for the strain expressing Module I from the GlucoBrick platform than for *P. putida* KT2440. Taken together, these results accredit the value of the rewired *P. putida* strains for the glucose-dependent biosynthesis of products derived from central carbon metabolism.

4. CONCLUSION

The metabolic lifestyle of *P. putida* has been evolutionary shaped by the environmental niches where this bacterium thrives. As such, it does not come as a surprise that the metabolic features of this species favor *diversity* (i.e. number and chemical nature of the substrates-to-be) over *efficiency* (i.e. energy yield per unit of carbon substrate consumed). Sugars are not readily processed by *P. putida*, and the metabolic network deployed for the consumption of hexoses is plagued by peripheral oxidation pathways in addition to a cyclic operation of catabolism (Nikel et al., 2015)—a feature shared by other *Pseudomonas* species (Wilkes et al., 2018). Time and again, examples of metabolic engineering approaches in the literature indicate that transforming the *identity* of central carbon metabolism in microorganisms is not an easy task (Jojima and Inui, 2015)—requiring a combination of rewiring the native biochemical network and tightly-controlled expression of genes encoding the intended catabolic functions. Reports describing approaches that target central carbon metabolism in general, and glycolysis in particular (which fuels bacterial cell factories to obtain energy and precursors needed for growth and bioproduction), are relatively scarce (Bogorad et al., 2013; Chen et al., 2013; Kannisto et al., 2014; Kern et al., 2007; Wang et

al., 2019). Manipulating the core metabolism of bacterial species, which is densely interconnected with the rest of the biochemical network and subjected to complex regulatory patterns, is thus a challenging aspect of metabolic engineering (Papagianni, 2012). However, the tools of contemporary synthetic biology allow for rationally designing alternative metabolic modules (*synthetic metabolism*) that can be plugged-in and -out of rewired bacterial *chassis* (Erb et al., 2017). By adopting this type of multi-factorial approach, Dvořák and de Lorenzo (2018) recently demonstrated how the range of carbohydrates used by *P. putida* can be broadened to include cellobiose and xylose—two substrates alien to the native catabolic scope of this bacterium. Along this line of reasoning, the present work shows how the catabolism of *P. putida* can be replaced by a rationally-designed glycolytic device. ^{13}C-Labelling experiments indicated that the engineered *P. putida* strain described herein generated the bulk of the Pyr pool from the EMP glycolytic route. If the objective is to maximize biomass yield from glucose, the activity and fluxes through the components of the novel metabolic module—as well as its connectivity with the background biochemical network—could be optimized *in vivo* through the evolutionary exploration of the solution space (Dragosits and Mattanovich, 2013; van den Bergh et al., 2018). The biosynthesis of secondary metabolite products derived from central carbon metabolism, on the other hand, can benefit from the approach undertaken in this study. Carotenoids could be accumulated to significantly higher levels in the engineered strains than in the wild-type (with a higher yield on the substrate), indicating that limited growth rates might be even an advantage for growth-uncoupled bioproduction.

Besides the biotechnological potential of such laboratory-created strains, the data above poses a legitimate question regarding the link between metabolic signatures (*metabolic lifestyle*) and species identity. The catabolism of sugars and other substrates has traditionally constituted one of the bases for taxonomic classification of bacterial isolates [e.g. in the early editions of the Bergey's *Manual of Systematic Bacteriology* (Buchanan and Gibbons, 1974)] before the onset of molecular markers such as the sequence of the gene encoding 16S RNA (van Belkum et al., 2001). The predominance of the ED pathway and the lack of Pfk have been considered typical metabolic signatures of Pseudomonads (Sokatch, 1986). The functional replacement of an archetypal biochemical network in a member of the group by a synthetic metabolism may also alter the factual taxonomy of the resulting bacterium. This type of deep metabolic engineering

applied to *P. putida* (and other bacteria) is likely to challenge the current frame for assigning a safety level to the corresponding species—and these developments certainly ask for novel criteria to deal with new-to-Nature biological agents. One way or the other, this work represents a first case example of what could be called *metabolic grafting* or *metabolic surgery* in *Pseudomonas*, and this approach could set the basis for further engineering whole-cell biocatalysts for different biotechnological purposes.

AUTHORS' CONTRIBUTIONS

A.S.P., L.F.C., V.D.L., and P.I.N. designed the experiments. V.D.L. and P.I.N. conceived the whole study and wrote the article. A.S.P. carried out genetic manipulations, quantitative physiology experiments, and *in vitro* enzyme assays. L.F.C. engineered and analyzed carotenoid biosynthesis in *P. putida*. All the authors contributed to the discussion of the research and interpretation of the data.

ACKNOWLEDGMENTS

This study was supported by grants from The Novo Nordisk Foundation (grant NNF10CC1016517, and *LiFe*, NNF18OC0034818) and the Danish Council for Independent Research (*SWEET*, DFF-Research Project 8021-00039B) to P.I.N. and by the HELIOS Project of the Spanish Ministry of Science BIO 2015-66960-C3-2-R (MINECO/FEDER); the ARISYS (ERC-2012-ADG-322797), EmPowerPutida (EU-H2020-BIOTEC-2014-2015-6335536), MADONNA (H2020-FET-OPEN-RIA-2017-1-766975), BioRoboost (H2020-NMBP-BIO-CSA-2018), and SYNBIO4FLAV (H2020-NMBP/0500) Contracts of the European Union and the S2017/BMD-3691 InGEMICS-CM funded by the Comunidad de Madrid (Spain) and the European Structural and Investment Funds. L.F.C. is supported by the European Union's Horizon 2020 Research and Innovation Programme under the Marie Skłodowska-Curie grant 713683 (*COFUNDfellowsDTU*). The authors declare that there are no competing interests associated with the contents of this article.

REFERENCES

Alves, A. M., Euverink, G. J., Bibb, M. J., Dijkhuizen, L., 1997. Identification of ATP-dependent phosphofructokinase as a regulatory step in the glycolytic pathway of the actinomycete *Streptomyces coelicolor* A3(2). Appl. Environ. Microbiol. 63**,** 956-961.

An, R., Moe, L. A., 2016. Regulation of pyrroloquinoline quinone-dependent glucose dehydrogenase activity in the model rhizosphere-dwelling bacterium *Pseudomonas putida* KT2440. Appl. Environ. Microbiol. 82**,** 4955-4964.

Arellano, B. H., Ortiz, J. D., Manzano, J., Chen, J. C., 2010. Identification of a dehydrogenase required for lactose metabolism in *Caulobacter crescentus*. Appl. Environ. Microbiol. 76**,** 3004-3014.

Bagdasarian, M., Lurz, R., Rückert, B., Franklin, F. C. H., Bagdasarian, M. M., Frey, J., Timmis, K. N., 1981. Specific purpose plasmid cloning vectors. II. Broad host range, high copy number, RSF1010-derived vectors, and a host-vector system for gene cloning in *Pseudomonas*. Gene. 16**,** 237-247.

Belda, E., van Heck, R. G. A., López-Sánchez, M. J., Cruveiller, S., Barbe, V., Fraser, C., Klenk, H. P., Petersen, J., Morgat, A., Nikel, P. I., Vallenet, D., Rouy, Z., Sekowska, A., Martins dos Santos, V. A. P., de Lorenzo, V., Danchin, A., Médigue, C., 2016. The revisited genome of *Pseudomonas putida* KT2440 enlightens its value as a robust metabolic *chassis*. Environ. Microbiol. 18**,** 3403-3424.

Benedetti, I., de Lorenzo, V., Nikel, P. I., 2016. Genetic programming of catalytic *Pseudomonas putida* biofilms for boosting biodegradation of haloalkanes. Metab. Eng. 33**,** 109-118.

Blank, L. M., Ionidis, G., Ebert, B. E., Bühler, B., Schmid, A., 2008. Metabolic response of *Pseudomonas putida* during redox biocatalysis in the presence of a second octanol phase. FEBS J. 275**,** 5173-5190.

Bogorad, I. W., Lin, T. S., Liao, J. C., 2013. Synthetic non-oxidative glycolysis enables complete carbon conservation. Nature. 502**,** 693-697.

Britton, G., Liaaen-Jensen, S., Pfander, H., 2004. Carotenoids. Birkhäuser, Basel, Switzerland.

Buchanan, R. E., Gibbons, N. R., 1974. Bergey's Manual of Determinative Bacteriology, 8th ed. Williams & Wilkins, Baltimore, MD, USA.

Buescher, J. M., Antoniewicz, M. R., Boros, L. G., Burgess, S. C., Brunengraber, H., Clish, C. B., DeBerardinis, R. J., Feron, O., Frezza, C., Ghesquiere, B., Gottlieb, E., Hiller, K., Jones, R. G., Kamphorst, J. J., Kibbey, R. G., Kimmelman, A. C., Locasale, J. W., Lunt, S. Y., Maddocks, O. D. K., Malloy, C., Metallo, C. M., Meuillet, E. J., Munger, J., Nöh, K., Rabinowitz, J. D., Ralser, M., Sauer, U., Stephanopoulos, G., St-Pierre, J., Tennant, D. A., Wittmann, C., Vander Heiden, M. G., Vazquez, A., Vousden, K., Young, J. D., Zamboni, N., Fendt, S.-M., 2015. A roadmap for interpreting ^{13}C metabolite labeling patterns from cells. Curr. Opin. Biotechnol. 34**,** 189-201.

Calero, P., Jensen, S. I., Nielsen, A. T., 2016. Broad-host-range *ProUSER* vectors enable fast characterization of inducible promoters and optimization of *p*-coumaric acid production in *Pseudomonas putida* KT2440. ACS Synth Biol. 5**,** 741-753.

Calero, P., Nikel, P. I., 2019. Chasing bacterial *chassis* for metabolic engineering: A perspective review from classical to non-traditional microorganisms. Microb. Biotechnol. 12**,** 98-124.

Chavarría, M., Goñi-Moreno, A., de Lorenzo, V., Nikel, P. I., 2016. A metabolic widget adjusts the phosphoenolpyruvate-dependent fructose influx in *Pseudomonas putida*. mSystems. 1**,** e00154-16.

Chavarría, M., Kleijn, R. J., Sauer, U., Pflüger-Grau, K., de Lorenzo, V., 2012. Regulatory tasks of the phosphoenolpyruvate-phosphotransferase system of *Pseudomonas putida* in central carbon metabolism. mBio. 3**,** e00028-12.

Chavarría, M., Nikel, P. I., Pérez-Pantoja, D., de Lorenzo, V., 2013. The Entner-Doudoroff pathway empowers *Pseudomonas putida* KT2440 with a high tolerance to oxidative stress. Environ. Microbiol. 15**,** 1772-1785.

Chen, R. R., Agrawal, M., Mao, Z., 2013. Impact of expression of EMP enzymes on glucose metabolism in *Zymomonas mobilis*. Appl. Biochem. Biotechnol. 170**,** 805-818.

Choi, K. H., Kumar, A., Schweizer, H. P., 2006. A 10-min method for preparation of highly electrocompetent *Pseudomonas aeruginosa* cells: application for DNA fragment transfer between chromosomes and plasmid transformation. J. Microbiol. Methods. 64**,** 391-397.

Corona, F., Martínez, J. L., Nikel, P. I., 2018. The global regulator Crc orchestrates the metabolic robustness underlying oxidative stress resistance in *Pseudomonas aeruginosa*. Environ. Microbiol. 21**,** 898-912.

Datsenko, K. A., Wanner, B. L., 2000. One-step inactivation of chromosomal genes in *Escherichia coli* K-12 using PCR products. Proc. Natl. Acad. Sci. USA. 97, 6640-6645.

de Lorenzo, V., Loza-Tavera, H., 2011. Microbial bioremediation of chemical pollutants: How bacteria cope with multi-stress environmental scenarios. In: Storz, G., Hengge, R. (Eds.), Bacterial Stress Responses, 2nd Edition. American Society of Microbiology, Washington D.C., pp. 481-492.

del Castillo, T., Duque, E., Ramos, J. L., 2008. A set of activators and repressors control peripheral glucose pathways in *Pseudomonas putida* to yield a common central intermediate. J. Bacteriol. 190, 2331-2339.

del Castillo, T., Ramos, J. L., Rodríguez-Herva, J. J., Fuhrer, T., Sauer, U., Duque, E., 2007. Convergent peripheral pathways catalyze initial glucose catabolism in *Pseudomonas putida*: Genomic and flux analysis. J. Bacteriol. 189, 5142-5152.

Dragosits, M., Mattanovich, D., 2013. Adaptive laboratory evolution – Principles and applications for biotechnology. Microb. Cell Fact. 12, 64.

Dvořák, P., de Lorenzo, V., 2018. Refactoring the upper sugar metabolism of *Pseudomonas putida* for co-utilization of cellobiose, xylose, and glucose. Metab. Eng. 48, 94-108.

Dvořák, P., Nikel, P. I., Damborský, J., de Lorenzo, V., 2017. *Bioremediation 3.0*: Engineering pollutant-removing bacteria in the times of systemic biology. Biotechnol. Adv. 35, 845-866.

Ebert, B. E., Kurth, F., Grund, M., Blank, L. M., Schmid, A., 2011. Response of *Pseudomonas putida* KT2440 to increased NADH and ATP demand. Appl. Environ. Microbiol. 77, 6597-6605.

Erb, T. J., Jones, P. R., Bar-Even, A., 2017. Synthetic metabolism: metabolic engineering meets enzyme design. Curr. Opin. Chem. Biol. 37, 56-62.

Flamholz, A., Noor, E., Bar-Even, A., Liebermeister, W., Milo, R., 2013. Glycolytic strategy as a tradeoff between energy yield and protein cost. Proc. Natl. Acad. Sci. USA. 110, 10039-10044.

Fuhrer, T., Fischer, E., Sauer, U., 2005. Experimental identification and quantification of glucose metabolism in seven bacterial species. J. Bacteriol. 187, 1581-1590.

Fürch, T., Preusse, M., Tomasch, J., Zech, H., Wagner-Döbler, I., Rabus, R., Wittmann, C., 2009. Metabolic fluxes in the central carbon metabolism of *Dinoroseobacter shibae* and

Phaeobacter gallaeciensis, two members of the marine *Roseobacter* clade. BMC Microbiol. 9, 209.

Green, M. R., Sambrook, J., 2012. Molecular cloning: a laboratory manual. Cold Spring Harbor Laboratory Press, Cold Spring Harbor, NY.

Hanahan, D., Meselson, M., 1983. Plasmid screening at high colony density. Methods Enzymol. 100, 333-342.

Heredia, V. V., Thomson, J., Nettleton, D., Sun, S., 2006. Glucose-induced conformational changes in glucokinase mediate allosteric regulation: Transient kinetic analysis. Biochemistry. 45, 7553-7562.

Hollinshead, W. D., Rodriguez, S., García-Martín, H., Wang, G., Baidoo, E. E. K., Sale, K. L., Keasling, J. D., Mukhopadhyay, A., Tang, Y. J., 2016. Examining *Escherichia coli* glycolytic pathways, catabolite repression, and metabolite channeling using Δ*pfk* mutants. Biotechnol. Biofuels. 9, 212.

Hunt, J. C., Phibbs, P. V., 1983. Regulation of alternate peripheral pathways of glucose catabolism during aerobic and anaerobic growth of *Pseudomonas aeruginosa*. J. Bacteriol. 154, 793-802.

Jiménez, J. I., Miñambres, B., García, J. L., Díaz, E., 2002. Genomic analysis of the aromatic catabolic pathways from *Pseudomonas putida* KT2440. Environ. Microbiol. 4, 824-841.

Jojima, T., Inui, M., 2015. Engineering the glycolytic pathway: A potential approach for improvement of biocatalyst performance. BioEngineered. 6, 328-334.

Kannisto, M., Aho, T., Karp, M., Santala, V., 2014. Metabolic engineering of *Acinetobacter baylyi* ADP1 for improved growth on gluconate and glucose. Appl. Environ. Microbiol. 80, 7021-7027.

Kern, A., Tilley, E., Hunter, I. S., Legisa, M., Glieder, A., 2007. Engineering primary metabolic pathways of industrial micro-organisms. J. Biotechnol. 129, 6-29.

Kim, S. H., Cavaleiro, A. M., Rennig, M., Nørholm, M. H., 2016. *SEVA Linkers*: A versatile and automatable DNA backbone exchange standard for Synthetic Biology. ACS Synth. Biol. 5, 1177-1181.

Klingner, A., Bartsch, A., Dogs, M., Wagner-Döbler, I., Jahn, D., Simon, M., Brinkhoff, T., Becker, J., Wittmann, C., 2015. Large-scale ^{13}C flux profiling reveals conservation of the Entner-

Doudoroff pathway as a glycolytic strategy among marine bacteria that use glucose. Appl. Environ. Microbiol. 81, 2408-2422.

Kohlstedt, M., Wittmann, C., 2019. GC-MS-based ^{13}C metabolic flux analysis resolves the parallel and cyclic glucose metabolism of *Pseudomonas putida* KT2440 and *Pseudomonas aeruginosa* PAO1. Metab. Eng. 54, 35-53.

Latrach-Tlemçani, L., Corroler, D., Barillier, D., Mosrati, R., 2008. Physiological states and energetic adaptation during growth of *Pseudomonas putida* mt-2 on glucose. Arch. Microbiol. 190, 141-150.

Lessie, T. G., Phibbs, P. V., 1984. Alternative pathways of carbohydrate utilization in pseudomonads. Annu. Rev. Microbiol. 38, 359-388.

Loeschcke, A., Markert, A., Wilhelm, S., Wirtz, A., Rosenau, F., Jaeger, K. E., Drepper, T., 2013. *TREX*: a universal tool for the transfer and expression of biosynthetic pathways in bacteria. ACS Synth. Biol. 2, 22-33.

Manoil, C., Beckwith, J., 1985. Tn*phoA*: a transposon probe for protein export signals. Proc. Natl. Acad. Sci. USA. 82, 8129-8133.

Martínez-García, E., Aparicio, T., de Lorenzo, V., Nikel, P. I., 2017. Engineering Gram-negative microbial cell factories using transposon vectors. Methods Mol. Biol. 1498, 273-293.

Martínez-García, E., de Lorenzo, V., 2011. Engineering multiple genomic deletions in Gram-negative bacteria: analysis of the multi-resistant antibiotic profile of *Pseudomonas putida* KT2440. Environ. Microbiol. 13, 2702-2716.

Martínez-García, E., de Lorenzo, V., 2017. Molecular tools and emerging strategies for deep genetic/genomic refactoring of *Pseudomonas*. Curr. Opin. Biotechnol. 47, 120-132.

Martins dos Santos, V. A. P., Heim, S., Moore, E. R., Strätz, M., Timmis, K. N., 2004. Insights into the genomic basis of niche specificity of *Pseudomonas putida* KT2440. Environ. Microbiol. 6, 1264-1286.

Matsushita, K., Shinagawa, E., Ameyama, M., 1982. D-Gluconate dehydrogenase from bacteria, 2-keto-D-gluconate-yielding, membrane-bound. Methods Enzymol. 89, 187-193.

Matsushita, K., Toyama, H., Adachi, O., 1994. Respiratory chains and bioenergetics of acetic acid bacteria. Adv. Microb. Physiol. 36, 247-301.

McIntire, W., Singer, T. P., Ameyama, M., Adachi, O., Matsushita, K., Shinagawa, E., 1985. Identification of the covalently bound flavins of D-gluconate dehydrogenases from

Pseudomonas aeruginosa and *Pseudomonas fluorescens* and of 2-keto-D-gluconate dehydrogenase from *Gluconobacter melanogenus*. Biochem. J. 231**,** 651-654.

Miller, B. G., Raines, R. T., 2004. Identifying latent enzyme activities: substrate ambiguity within modern bacterial sugar kinases. Biochemistry. 43**,** 6387-6392.

Misawa, N., Nakagawa, M., Kobayashi, K., Yamano, S., Izawa, Y., Nakamura, K., Harashima, K., 1990. Elucidation of the *Erwinia uredovora* carotenoid biosynthetic pathway by functional analysis of gene products expressed in *Escherichia coli*. J. Bacteriol. 172**,** 6704-6712.

Nanchen, A., Fuhrer, T., Sauer, U., 2007. Determination of metabolic flux ratios from ^{13}C-experiments and gas chromatography-mass spectrometry data: protocol and principles. Methods Mol. Biol. 358**,** 177-197.

Nelson, K. E., Weinel, C., Paulsen, I. T., Dodson, R. J., Hilbert, H., Martins dos Santos, V. A. P., Fouts, D. E., Gill, S. R., Pop, M., Holmes, M., Brinkac, L., Beanan, M., DeBoy, R. T., Daugherty, S., Kolonay, J., Madupu, R., Nelson, W., White, O., Peterson, J., Khouri, H., Hance, I., Chris Lee, P., Holtzapple, E., Scanlan, D., Tran, K., Moazzez, A., Utterback, T., Rizzo, M., Lee, K., Kosack, D., Moestl, D., Wedler, H., Lauber, J., Stjepandic, D., Hoheisel, J., Straetz, M., Heim, S., Kiewitz, C., Eisen, J. A., Timmis, K. N., Düsterhöft, A., Tümmler, B., Fraser, C. M., 2002. Complete genome sequence and comparative analysis of the metabolically versatile *Pseudomonas putida* KT2440. Environ. Microbiol. 4**,** 799-808.

Nikel, P. I., Chavarría, M., 2016. Quantitative physiology approaches to understand and optimize reducing power availability in environmental bacteria. In: McGenity, T. J., Timmis, K. N., Nogales-Fernández, B. (Eds.), Hydrocarbon and Lipid Microbiology Protocols–Synthetic and Systems Biology - Tools. Humana Press, Heidelberg, Germany, pp. 39-70.

Nikel, P. I., Chavarría, M., Danchin, A., de Lorenzo, V., 2016. From dirt to industrial applications: *Pseudomonas putida* as a Synthetic Biology *chassis* for hosting harsh biochemical reactions. Curr. Opin. Chem. Biol. 34**,** 20-29.

Nikel, P. I., Chavarría, M., Fuhrer, T., Sauer, U., de Lorenzo, V., 2015. *Pseudomonas putida* KT2440 strain metabolizes glucose through a cycle formed by enzymes of the Entner-Doudoroff, Embden-Meyerhof-Parnas, and pentose phosphate pathways. J. Biol. Chem. 290**,** 25920-25932.

Nikel, P. I., de Lorenzo, V., 2013a. Implantation of unmarked regulatory and metabolic modules in Gram-negative bacteria with specialised mini-transposon delivery vectors. J. Biotechnol. 163, 143-154.

Nikel, P. I., de Lorenzo, V., 2013b. Engineering an anaerobic metabolic regime in *Pseudomonas putida* KT2440 for the anoxic biodegradation of 1,3-dichloroprop-1-ene. Metab. Eng. 15, 98-112.

Nikel, P. I., de Lorenzo, V., 2018. *Pseudomonas putida* as a functional *chassis* for industrial biocatalysis: From native biochemistry to *trans*-metabolism. Metab. Eng. 50, 142-155.

Nikel, P. I., Kim, J., de Lorenzo, V., 2014a. Metabolic and regulatory rearrangements underlying glycerol metabolism in *Pseudomonas putida* KT2440. Environ. Microbiol. 16, 239-254.

Nikel, P. I., Martínez-García, E., de Lorenzo, V., 2014b. Biotechnological domestication of pseudomonads using synthetic biology. Nat. Rev. Microbiol. 12, 368-379.

Nikel, P. I., Pérez-Pantoja, D., de Lorenzo, V., 2013. Why are chlorinated pollutants so difficult to degrade aerobically? Redox stress limits 1,3-dichloroprop-1-ene metabolism by *Pseudomonas pavonaceae*. Philos. Trans. R. Soc. Lond. B Biol. Sci. 368, 20120377.

Nikel, P. I., Zhu, J., San, K. Y., Méndez, B. S., Bennett, G. N., 2009. Metabolic flux analysis of *Escherichia coli creB* and *arcA* mutants reveals shared control of carbon catabolism under microaerobic growth conditions. J. Bacteriol. 191, 5538-5548.

Nour-Eldin, H. H., Geu-Flores, F., Halkier, B. A., 2010. *USER* cloning and *USER* fusion: The ideal cloning techniques for small and big laboratories. Methods Mol. Biol. 643, 185-200.

Papagianni, M., 2012. Recent advances in engineering the central carbon metabolism of industrially important bacteria. Microb. Cell Fact. 11, 50.

Peekhaus, N., Conway, T., 1998. What's for dinner?: Entner-Doudoroff metabolism in *Escherichia coli*. J. Bacteriol. 180, 3495-3502.

Poblete-Castro, I., Wittmann, C., Nikel, P. I., 2019. Biochemistry, genetics, and biotechnology of glycerol utilization in *Pseudomonas* species. Microb. Biotechnol., In press, DOI: 10.1111/1751-7915.13400.

Ruiz, J. A., Fernández, R. O., Nikel, P. I., Méndez, B. S., Pettinari, M. J., 2006. *dye* (*arc*) Mutants: insights into an unexplained phenotype and its suppression by the synthesis of poly(3-hydroxybutyrate) in *Escherichia coli* recombinants. FEMS Microbiol. Lett. 258, 55-60.

Sánchez-Pascuala, A., de Lorenzo, V., Nikel, P. I., 2017. Refactoring the Embden-Meyerhof-Parnas pathway as a whole of portable GlucoBricks for implantation of glycolytic modules in Gram-negative bacteria. ACS Synth. Biol. 6**,** 793-805.

Sánchez-Pascuala, A., Nikel, P. I., de Lorenzo, V., 2018. Re-factoring glycolytic genes for targeted engineering of catabolism in Gram-negative bacteria. In: Braman, J. C. (Ed.), Synthetic Biology: Methods and protocols. Springer New York, New York, NY, pp. 3-24.

Sandmann, G., 2015. Carotenoids of biotechnological importance. Adv. Biochem. Eng. Biotechnol. 148**,** 449-467.

Schweiggert, R. M., Carle, R., 2016. Carotenoid production by bacteria, microalgae, and fungi. In: Kaczor, A., Baranska, M. (Eds.), Carotenoids: Nutrition, analysis and technology. Wiley-Blackwell, Oxford, UK, pp. 217-240.

Silva-Rocha, R., Martínez-García, E., Calles, B., Chavarría, M., Arce-Rodríguez, A., de las Heras, A., Páez-Espino, A. D., Durante-Rodríguez, G., Kim, J., Nikel, P. I., Platero, R., de Lorenzo, V., 2013. The Standard European Vector Architecture (SEVA): a coherent platform for the analysis and deployment of complex prokaryotic phenotypes. Nucleic Acids Res. 41**,** D666-D675.

Sokatch, J. R., 1986. The biology of *Pseudomonas*. Academic Press, Boston, MS, USA.

Stutz, H., Bresgen, N., Eckl, P. M., 2015. Analytical tools for the analysis of β-carotene and its degradation products. Free Rad. Res. 49**,** 650-680.

Sudarsan, S., Dethlefsen, S., Blank, L. M., Siemann-Herzberg, M., Schmid, A., 2014. The functional structure of central carbon metabolism in *Pseudomonas putida* KT2440. Appl. Environ. Microbiol. 80**,** 5292-5303.

Szyperski, T., 1995. Biosynthetically directed fractional ^{13}C-labeling of proteinogenic amino acids: An efficient analytical tool to investigate intermediary metabolism. Eur. J. Biochem. 232**,** 433-448.

Vallenet, D., Calteau, A., Cruveiller, S., Gachet, M., Lajus, A., Josso, A., Mercier, J., Renaux, A., Rollin, J., Rouy, Z., Roche, D., Scarpelli, C., Médigue, C., 2017. MicroScope in 2017: an expanding and evolving integrated resource for community expertise of microbial genomes. Nucleic Acids Res. 45**,** D517-D528.

van Belkum, A., Struelens, M., de Visser, A., Verbrugh, H., Tibayrenc, M., 2001. Role of genomic typing in taxonomy, evolutionary genetics, and microbial epidemiology. Clin. Microbiol. Rev. 14, 547-560.

van den Bergh, B., Swings, T., Fauvart, M., Michiels, J., 2018. Experimental design, population dynamics, and diversity in microbial experimental evolution. Microbiol. Mol. Biol. Rev. 82.

van der Werf, M. J., Overkamp, K. M., Muilwijk, B., Koek, M. M., van der Werff-van der Vat, B. J., Jellema, R. H., Coulier, L., Hankemeier, T., 2008. Comprehensive analysis of the metabolome of *Pseudomonas putida* S12 grown on different carbon sources. Mol. BioSyst. 4, 315-327.

Vicente, M., Cánovas, J. L., 1973a. Regulation of the glucolytic enzymes in *Pseudomonas putida*. Arch. Microbiol. 93, 53-64.

Vicente, M., Cánovas, J. L., 1973b. Glucolysis in *Pseudomonas putida*: physiological role of alternative routes from the analysis of defective mutants. J. Bacteriol. 116, 908-914.

Wang, Q., Xu, J., Sun, Z., Luan, Y., Li, Y., Wang, J., Liang, Q., Qi, Q., 2019. Engineering an *in vivo* EP-bifido pathway in *Escherichia coli* for high-yield acetyl-CoA generation with low CO_2 emission. Metab. Eng. 51, 79-87.

Wilkes, R. A., Mendonca, C. M., Aristilde, L., 2018. A cyclic metabolic network in *Pseudomonas protegens* Pf-5 prioritizes the Entner-Doudoroff pathway and exhibits substrate hierarchy during carbohydrate co-utilization. Appl. Environ. Microbiol. 85, e02084-18.

Winsor, G. L., Griffiths, E. J., Lo, R., Dhillon, B. K., Shay, J. A., Brinkman, F. S., 2016. Enhanced annotations and features for comparing thousands of *Pseudomonas* genomes in the *Pseudomonas* Genome Database. Nucleic Acids Res. 44, D646-D653.

Wirth, N. T., Kozaeva, E., Nikel, P. I., 2019. Accelerated genome engineering of *Pseudomonas putida* by I-*Sce*I—mediated recombination and CRISPR-Cas9 counterselection. Microb. Biotechnol., In press, DOI: 10.1111/1751-7915.13396.

Worsey, M. J., Williams, P. A., 1975. Metabolism of toluene and xylenes by *Pseudomonas putida* (*arvilla*) mt-2: evidence for a new function of the TOL plasmid. J. Bacteriol. 124, 7-13.

Yu, S., Lai, B., Plan, M. R., Hodson, M. P., Lestari, E. A., Song, H., Krömer, J. O., 2018. Improved performance of *Pseudomonas putida* in a bioelectrochemical system through overexpression of periplasmic glucose dehydrogenase. Biotechnol. Bioeng. 115, 145-155.

Zhao, J., Li, Q., Sun, T., Zhu, X., Xu, H., Tang, J., Zhang, X., Ma, Y., 2013. Engineering central metabolic modules of *Escherichia coli* for improving β-carotene production. Metab. Eng. 17, 42-50.

TABLES

Table 1. Bacterial strains used in this study.

Strain	Relevant characteristics[a]	Reference or source
Escherichia coli		
CC118	Cloning host; Δ(*ara-leu*) *araD* Δ*lacX174 galE galK phoA thiE1 rpsE rpoB*(Rif^R) *argE*(Am) *recA1*	Manoil and Beckwith (1985)
DH5α λ*pir*	Cloning host; F$^-$ λ$^-$ *endA1 glnX44*(AS) *thiE1 recA1 relA1 spoT1 gyrA96*(Nal^R) *rfbC1 deoR nupG* Φ80(*lacZ*Δ*M15*) Δ(*argF-lac*)*U169 hsdR17*(r_K^- m_K^+), λ*pir* lysogen	Hanahan and Meselson (1983)
BW25113[b]	Wild-type strain; F$^-$ λ$^-$ Δ(*araD-araB*)*567* Δ*lacZ4787*(::*rrnB-3*) *rph-1* Δ(*rhaD-rhaB*)*568 hsdR514*	Datsenko and Wanner (2000)
BPfkAB	Same as BW25113, but Δ*pfkA775*::*FRT* Δ*pfkB722*::*aphA*; Km^R	Sánchez-Pascuala et al. (2017)
BPG	Same as BW25113, but Δ*glk-726*::*FRT* Δ*ptsI745*::*aphA*; Km^R	Nikel and de Lorenzo (2013a)
Pseudomonas putida		
KT2440	Wild-type strain, derived from *P. putida* mt-2 (Worsey and Williams, 1975) cured of the TOL plasmid pWW0	Bagdasarian et al. (1981)
KT2440 Δ*glk*	Same as KT2440, but with an in-frame deletion of the *glk* gene (*PP_1011*)	Sánchez-Pascuala et al. (2017)
KT2440 Δ*gcd*	Same as KT2440, but with an in-frame deletion of the *gcd* gene (*PP_1444*)	This study
KT2440 Δ*PP_3382-4*	Same as KT2440, but with an in-frame deletion of the genes *PP_3382*, *PP_3383* and *PP_3384* by a single deletion event	This study
KT2440 Δ*PP_3623*	Same as KT2440, but with an in-frame deletion of the *PP_3623* gene	This study
KT2440	Same as KT2440, but with an in-frame deletion of the	This study

Δ*PP_4232*	*PP_4232* gene	
KT2440 Δ*gad*	Same as KT2440 Δ*PP_3382-4*, but with an in-frame deletion of the genes *PP_3623* and *PP_4232*	This study
KT2440 Δ*edd*	Same as KT2440, but with an in-frame deletion of the *edd* gene (*PP_1010*)	This study
GC1	Glycolytic *chassis* I; derivative of *P. putida* KT2440 with the deletions described for the mutants Δ*glk,* Δ*gcd,* Δ*gad* and Δ*edd*	This study

[a] Antibiotic markers: *Km*, kanamycin; *Nal*, nalidixic acid; and *Rif*, rifampicin.

[b] Strain obtained from the *E. coli* Genetic Stock Center (Yale University, New Haven, CT, USA).

Table 2. Metabolomic determinations[a] in wild-type and engineered *P. putida* strains grown in glucose cultures.

***P. putida* strain/plasmid**	**Intracellular content** (nmol mg_{CDW}^{-1}) **of**				
	Glucose-6-*P*	Fructose-6-*P*	Dihydroxyacetone-*P*	Glyceraldehyde-3-*P*	Pyruvate
KT2440/pSEVA224 (empty vector)	52 ± 9[b]	3.8 ± 0.2	1.4 ± 0.2	0.39 ± 0.08[b]	1.1 ± 0.4
GC1/pS224·GBI (Module I)	73 ± 6	5.4 ± 0.2	2.2 ± 0.3	0.85 ± 0.05	3.1 ± 0.5

[a] Cells were grown aerobically in M9 minimal medium added with glucose at 20 mM as the sole carbon source and IPTG at 1 mM, harvested during exponential growth, and rapidly quenched with liquid N_2. Intracellular metabolites were extracted and their concentration determined by means of liquid chromatography coupled to mass spectrometry. Each parameter is reported as the mean value ± standard deviation from duplicate measurements in at least two independent experiments. CDW, cell dry weight.

[b] Values obtained from Sánchez-Pascuala et al. (2017).

FIGURES

Figure 1 · Predominant glycolytic regimes in bacterial species and engineering strategies. (a) Glucose catabolism occurs mainly through the activity of the Embden-Meyerhof-Parnas (EMP) or the Entner-Doudoroff (ED) pathway, which differ both in the metabolic architecture of the route and the ATP yield on substrate (Flamholz et al., 2013; Nikel et al., 2016). The abbreviations used in this diagram are as follows: G6P, glucose-6-*P*; FBP, fructose-1,6-P_2; KDPG, 2-keto-3-deoxy-6-phosphogluconate; GA3P, glyceraldehyde-3-*P*; Pyr, pyruvate; and P_i, inorganic phosphate. Note that some reactions have been lumped for the sake of simplicity. **(b)** Schematic representation of GlucoBricks, a synthetic biology platform for engineering glycolysis in Gram-negative bacteria (Sánchez-Pascuala et al., 2017). In plasmid pS224·GBI, the glycolytic genes encoding the enzymes of the preparatory phase of the EMP pathway (i.e. module I) are placed under the transcriptional control of an inducible $LacI^Q/P_{trc}$ element as a single transcriptional unit flanked by *Avr*II and *Bam*HI restriction sites. Each gene is preceded by a synthetic regulatory element, indicated by a purple circle, composed of a ribosome binding site and a short spacer sequence (5'-AGG AGG AAA AAC AT-3').

Figure 2 · Schematic representation of the central carbon metabolism in *P. putida* KT2440. Glucose catabolism in this species occurs mainly through the activity of the Entner-Doudoroff (ED) pathway, and part of the trioses-*P* thereby generated are recycled back to hexoses-*P* by means of the *EDEMP cycle* (shaded in blue), that also encompasses activities from the Embden-Meyerhof-Parnas (EMP) and pentose phosphate (PP) pathways. Note that a set of *peripheral reactions* can also oxidize glucose to gluconate and/or 2-ketogluconate (2KG) before any phosphorylation of the intermediates occurs. Each metabolism block is indicated with a different color, and catabolism downward acetyl-coenzyme A (CoA) is indicated by a wide gray arrow. Note that 6-phosphofructo-1-kinase (Pfk) activity is absent in the network, as indicated as a dashed grey row close to the gluconeogenic Fbp reaction. The abbreviations used in this diagram are as follows: G6P, glucose-6-*P*; F6P, fructose-6-*P*; FBP, fructose-1,6-P_2; DHAP, dihydroxyacetone-*P*; GA3P, glyceraldehyde-3-*P*; BPG, glycerate-1,3-P_2; 3PG, glycerate-3-*P*; 2PG, glycerate-2-*P*; PEP, phosphoenolpyruvate; Pyr, pyruvate; 6PG, 6-phosphogluconate; KDPG, 2-keto-3-deoxy-6-phosphogluconate; 2K6PG, 2-ketogluconate-6-*P*; OM, outer membrane; PS, periplasmic space; and IM, inner membrane.

Figure 3 · Phenotypic characterization of the *glk* and *gcd* deletion in *P. putida* KT2440. (a) *In vitro* quantification of the specific (Sp) glucokinase (Glk) and glucose dehydrogenase (Gcd) activity in wild-type (WT) *P. putida* KT2440, and its Δ*glk* and Δ*gcd* mutant derivatives. All strains were grown on M9 minimal medium added with glucose at 20 mM and cells were harvested in mid-exponential phase to obtain cell-free extracts. Each bar represents the mean value of the corresponding enzyme activity ± standard deviation of quadruplicate measurements from at least two independent experiments. Significant differences ($P < 0.05$, as evaluated by means of the Student's *t* test) in the pair-wise comparison of a given recombinant to the control WT strain are indicated by an asterisk. **(b)** Growth curves of *P. putida* KT2440 and its Δ*glk* and Δ*gcd* derivative under glycolytic (M9 minimal medium with glucose) or gluconeogenic (M9 minimal medium with succinate) conditions. Each data point represents the mean value of the optical density measured at 600 nm (OD_{600}) of quadruplicate measurements from at least three independent experiments. The specific growth rates (μ) were calculated from these data during exponential growth, and the inset shows the mean values ± standard deviations for each strain. The abbreviations used in this diagram are as follows: G6P, glucose-6-*P*; and PQQ, (redox cofactor) pyrroloquinoline quinone.

Figure 4 · Phenotypic characterization of the *gad* deletions in *P. putida* KT2440. (a) Distribution of hypothetical genes in the chromosome of *P. putida* KT2440 encoding gluconate 2-dehydrogenase (Gad) activity. The relative orientation of the genes in the chromosome is likewise indicated. FAD, flavin adenine dinucleotide. **(b)** *In vitro* quantification of the specific (Sp) Gad activity in wild-type (WT) *P. putida* KT2440, and the mutant strains Δ*PP_3382-4* (which comprises the deletions of *PP_3382*, *PP_3383*, and *PP_3384*), Δ*PP_3623*, Δ*PP_4232*, and Δ*gad* (which comprises the deletions from Δ*PP_3382-4*, Δ*PP_3623*, and Δ*PP_4232*). All strains were grown on M9 minimal medium added with glucose at 20 mM and cells were harvested in mid-exponential phase to obtain cell-free extracts. Each bar represents the mean value of the corresponding enzyme activity ± standard deviation of quadruplicate measurements from at least two independent experiments. Significant differences ($P < 0.05$, as evaluated by means of the Student's *t* test) in the pair-wise comparison of a given recombinant to the control WT strain are indicated by an asterisk. (c) Growth curves of *P. putida* KT2440 and *gad* mutants under glycolytic (M9 minimal medium with glucose) or gluconeogenic (M9 minimal medium with succinate) conditions. Each data point represents the mean value of the optical density measured at 600 nm (OD_{600}) of quadruplicate measurements from at least three independent experiments. The specific growth rates (μ) were calculated from these data during exponential growth, and the inset shows the mean values ± standard deviations for each strain.

Figure 5 · Growth phenotype characterization of different glucose catabolism mutants of *P. putida* KT2440. M9 minimal medium plates, containing either 20 mM glucose (left plate) or 30 mM succinate (right plate), were seeded with *P. putida* KT2440 (wild-type) and the mutants Δ*glk* (PP_1011, glucokinase), Δ*gcd* (PP_1444, glucose dehydrogenase), Δ*glk* Δ*gcd*, Δ*gad* (which comprises the deletions of Δ*PP_3382*, Δ*PP_3383*, Δ*PP_3384*, Δ*PP_3623* and Δ*PP_4232*, encoding gluconate 2-dehydrogenase), and Δ*edd* (PP_1010, 6-phosphogluconate dehydratase), and incubated for 36 h at 30°C. The phenotypes of the strains are indicated as "+" (growth) and "–" (no growth). The values in parentheses indicate the normalized growth coefficient, which represents the fraction of the specific growth rate attained by the mutant strain when compared to that of the wild-type under the same culture conditions. Significant differences ($P < 0.05$, as evaluated by means of the Student's *t* test) in the comparison of the normalized growth coefficient between a given mutant and *P. putida* KT2440 are indicated in red.

Figure 6 · Engineering a EMP-based glycolytic route in *P. putida* GC1. (a) Simplified representation of central carbon metabolism in *P. putida* GC1 (glycolytic *chassis* I) upon implantation of the synthetic glycolysis. The metabolic activities eliminated in this strain are represented by dashed red arrows, the biochemical reactions encoded by the genes within Module I of the GlucoBrick platform are indicated in purple, and endogenous reactions are shown in gray. Reactions converting GA3P into pyruvate are lumped. The abbreviations used in this diagram are as indicated in Fig. 2. **(b)** M9 minimal medium plates, containing either 20 mM glucose (left column) or 30 mM succinate (right column), were inoculated with *P. putida* KT2440 (WT) carrying the empty pSEVA224 vector, and *P. putida* GC1 carrying either the empty pSEVA224 vector or GlucoBrick Module I (pS224·GBI, see also Fig. 1b) and incubated for 36 h at 30°C. Culture medium additives (Km, kanamycin; and IPTG, isopropyl-1-thio-β-galactopyranoside) are likewise indicated. **(c)** Growth curves of *P. putida* KT2440 carrying the empty pSEVA224 vector, and *P. putida* GC1 carrying plasmid pS224·GBI on M9 minimal medium with 20 mM glucose, 50 μg ml^{-1} Km, and 1 mM IPTG in microtiter-plate cultures. Each data point in the growth curves represents the mean value of the optical density measured at 600 nm (OD_{600}) in quadruplicate measurements from at least three independent experiments. The specific growth rates (μ) were calculated from these data during exponential growth, and the inset shows the mean value ± standard deviations for each strain.

Figure 7 · Physiological and biochemical characterization of the designed EMP glycolytic device in *P. putida* GC1. (a) *In vitro* quantification of the specific (Sp) glucokinase (Glk) activity in wild-type (WT) *E. coli* BW25113 and its Δ*glk* Δ*ptsI* derivative, and in *P. putida* KT2440 (WT) and its Δ*glk* derivative (left panel) carrying the empty pSEVA224 vector. The right panel shows the Glk activity measurements in *P. putida* GC1 carrying plasmid pS224·GBI. **(b)** *In vitro* quantification of the Sp 6-phosphofructo-1-kinase (Pfk) activity in WT *E. coli* BW25113 and its Δ*pfkA* Δ*pkfB* derivative (termed Δ*pfk*), and in *P. putida* KT2440 (WT, left panel) carrying the empty pSEVA224 vector. The right panel shows the Pfk activity for *P. putida* GC1 carrying plasmid pS224·GBI. **(c)** Glucose consumption profiles of *P. putida* KT2440 and GC1 carrying either the control vector (pSEVA224) or pS224·GBI. All strains were grown on M9 minimal medium with 20 mM glucose, 50 μg ml^{-1} Km, and 1 mM IPTG, and cells were harvested in mid-exponential phase to obtain cell-free extracts and cell dry weight (CDW). Note that *P. putida* GC1/pS224·GBI was compared to *P. putida* Δ*glk* for Glk activity, and to *P. putida* KT2440 for Pfk activity. Each bar represents the mean value of the corresponding parameter ± standard deviation of quadruplicate measurements from at least two independent experiments. Significant differences ($P < 0.05$, as evaluated by means of the Student's *t* test) in the pair-wise comparison of a given recombinant to the control strain are indicated by an asterisk.

Figure 8 · Assessment of the metabolic origin of glycolytic intermediates in engineered *P. putida* using ^{13}C-labelled substrates. (a) Glucose-6-*P*, a hub metabolite in the upper metabolism of *P. putida*, can be transformed into pyruvate (Pyr) by means of the Entner-Doudoroff (ED), Embden-Meyerhof-Parnas (EMP), or pentose phosphate (PP) pathways. The expected labelling pattern of individual Pyr molecules is indicated for each processing route. **(b)** Positional ^{13}C enrichment of trioses enables tracing the metabolic origin of the Pyr pool. *P. putida* KT2440 (WT) carrying the empty pSEVA224 vector and *P. putida* GC1 carrying plasmid pS224·GBI were grown on M9 minimal medium with 20 mM [1-$^{13}C_1$]-glucose, and the biomass was harvested in mid-exponential phase to process samples for GC-MS analysis. **(c)** *In vitro* quantification of the specific (Sp) 6-phoshogluconate (6PG) dehydratase activity (Edd), first step of the ED pathway [6-phosphogluconate (6PG) → 2-keto-3-deoxy-6-phosphogluconate (KDPG)], in *P. putida* KT2440 (WT) and GC1. KDPG aldolase (Eda) subsequently splits KDPG into glyceraldehyde-3-*P* (GA3P) and Pyr. Strains were grown on M9 minimal medium with 20 mM glucose and cells were harvested in mid-exponential phase to obtain cell-free extracts. Each bar represents the mean Edd activity value ± standard deviation of quadruplicate measurements from at least two independent experiments. Significant differences ($P < 0.01$, as evaluated by means of the Student's *t* test) in the pair-wise comparison are indicated by an asterisk.

Figure 9 · Engineered *P. putida* strains running a synthetic glycolysis display enhanced carotenoid synthesis from glucose. (a) Scheme of the *crt* gene cluster from *Pantoea ananatis*, expressed from a XylS/*Pm* regulatory element in plasmid pS1·CRT. RBS, ribosome binding site. **(b)** Carotenoid synthesis pathway. The key intermediate FPP is transformed into β-carotene *via* the MEP pathway and the heterologous carotenoid pathway, which includes the sequential action of the CrtE, CrtB, CrtI, and CrtY components. The abbreviations used in this diagram are as follows: GA3P, glyceraldehyde-3-*P*; HMBPP, 4-hydroxy-3-methylbut-2-enyl pyrophosphate; IPP, isopentenyl pyrophosphate; DMAPP, dimethylallyl pyrophosphate; FPP, farnesyl pyrophosphate; GGPP, geranylgeranyl pyrophosphate; and MEP pathway, methylerythritol 4-phosphate pathway. Note that the number of carbon atoms in each metabolite is given in parentheses, and dashed lines represent multiple biochemical steps. **(c)** Analysis of carotenoid synthesis in wild-type and engineered *P. putida* cells. Wild-type (WT) strain KT2440 and *P. putida* GC1, containing Module I of the GlucoBrick platform (GBI), were transformed either with an empty pPS1 vector or plasmid pPS1·CRT (carrying the *crt* genes). All the resulting engineered strains were grown on M9 minimal medium with 20 mM glucose (and antibiotics and inducers as appropriate), and cells were harvested 24-h post-induction of the expression of genes encoding the carotenoid pathway. The carotenoid content, glucose consumption, and cell dry weight (CDW) concentration were analyzed in all the samples, and the mass yield of carotenoid on sugar ($Y_{carotenoid/glucose}$) was calculated from these values. A representative picture of the engineered strains, plated on M9 minimal medium containing glucose and incubated at 30°C for 48 h, is shown at the bottom of the figure. Bars represent mean values ± standard deviation of triplicate measurements from at least two independent experiments. Significant differences ($P < 0.05$, as evaluated by means of the Student's *t* test) in pair-wise comparisons are indicated by an asterisk. N.D., not detected (i.e. control experiments, in which the corresponding strains carry an empty pPS1 vector).

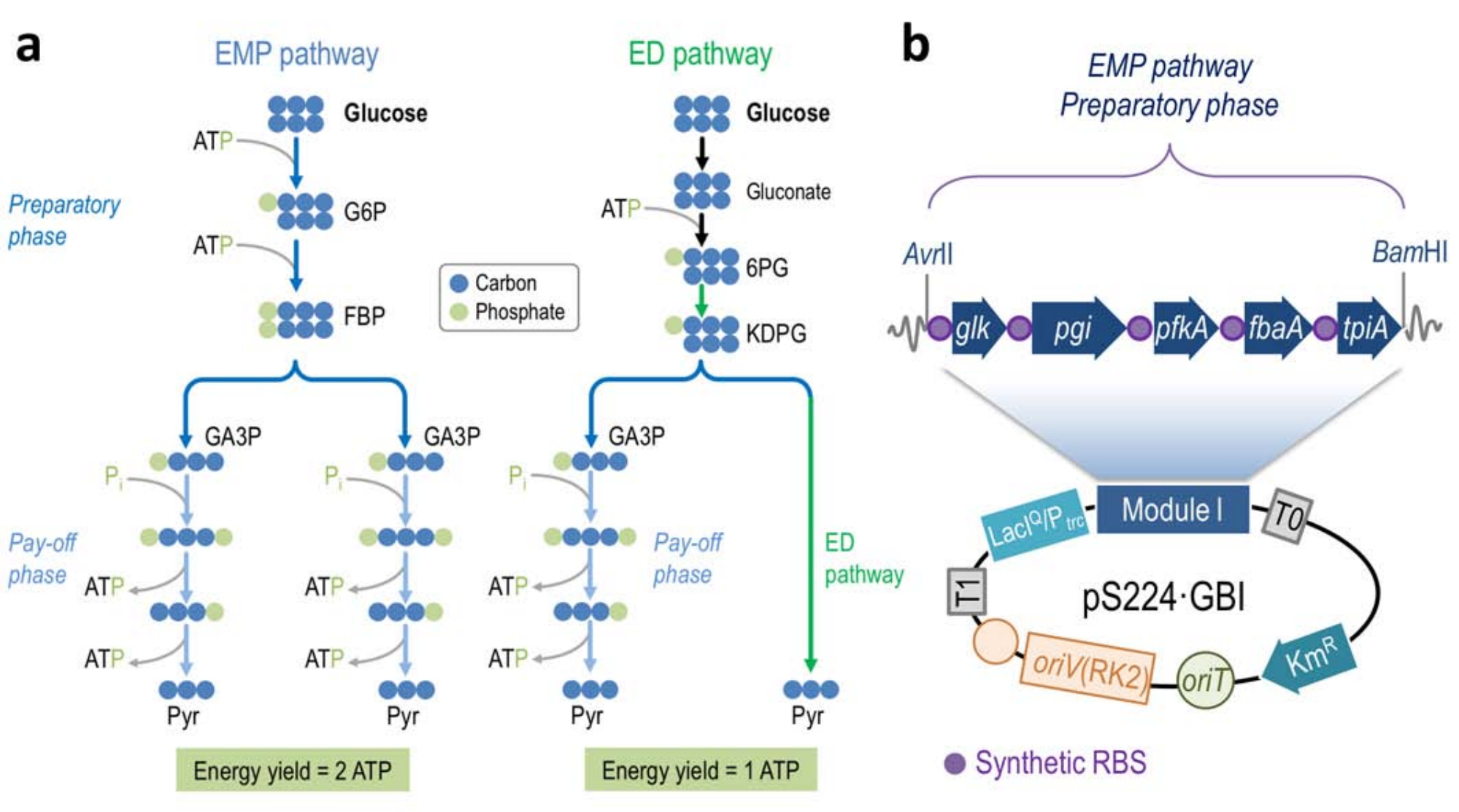
a
EMP pathway
ED pathway
Glucose
ATP
G6P
ATP
FBP
Preparatory phase
Carbon
Phosphate
Glucose
Gluconate
ATP
6PG
KDPG
GA3P
GA3P
GA3P
Pi
Pi
Pi
Pay-off phase
ATP
ATP
ATP
ATP
ATP
ATP
Pay-off phase
ED pathway
Pyr
Pyr
Pyr
Pyr
Energy yield = 2 ATP
Energy yield = 1 ATP
b
EMP pathway
Preparatory phase
AvrII
BamHI
glk
pgi
pfkA
fbaA
tpiA
LacIQ/Ptrc
Module I
T0
T1
pS224·GBI
oriV(RK2)
oriT
KmR
Synthetic RBS

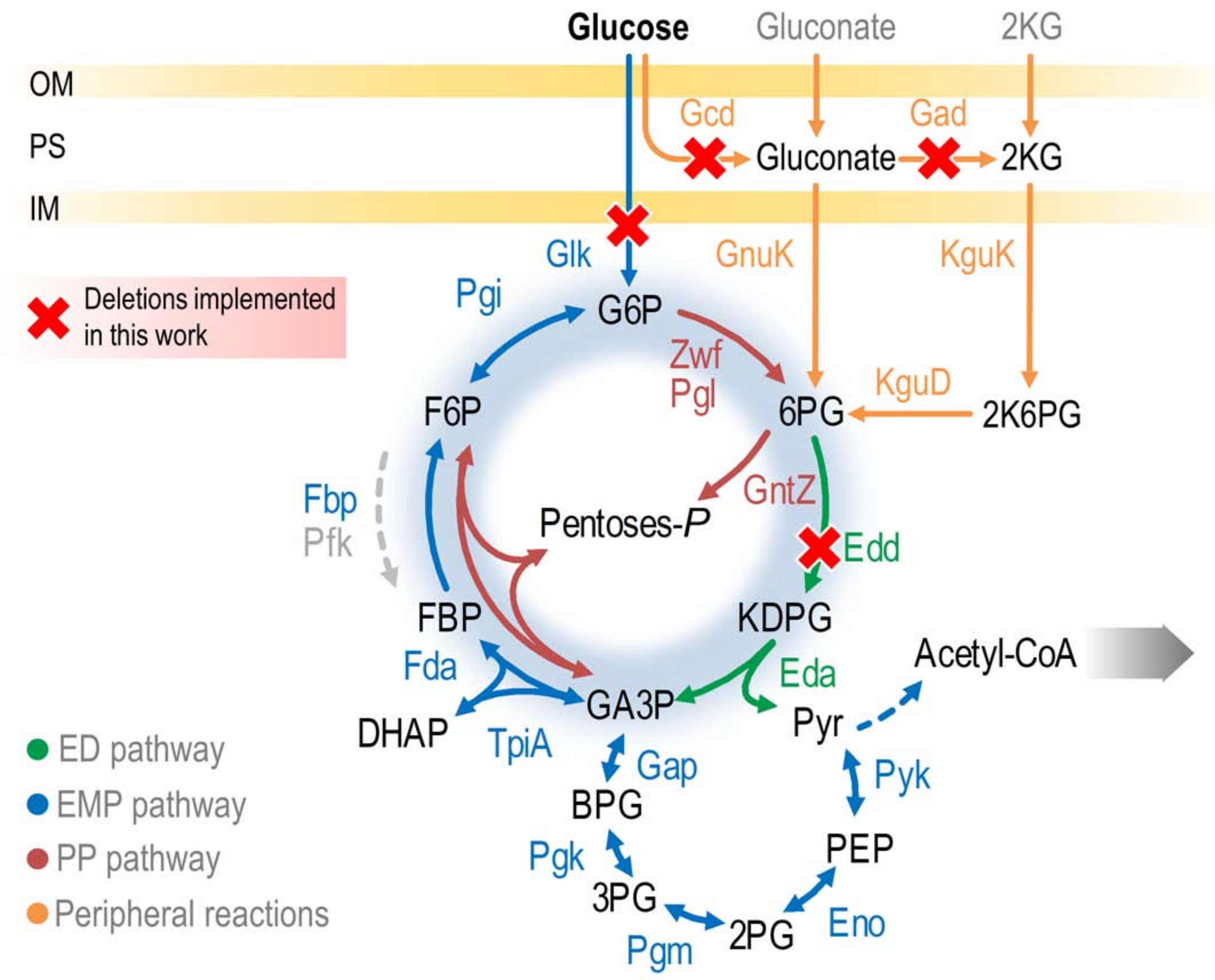
Glucose
Gluconate
2KG
OM
PS
IM
Gcd
Gad
Gluconate
2KG
Glk
GnuK
KguK
Deletions implemented in this work
Pgi
G6P
Zwf
Pgl
KguD
F6P
6PG
2K6PG
Fbp
Pfk
GntZ
Pentoses-P
Edd
FBP
KDPG
Acetyl-CoA
Fda
Eda
GA3P
Pyr
DHAP
TpiA
Gap
Pyk
BPG
PEP
Pgk
3PG
2PG
Eno
Pgm
ED pathway
EMP pathway
PP pathway
Peripheral reactions

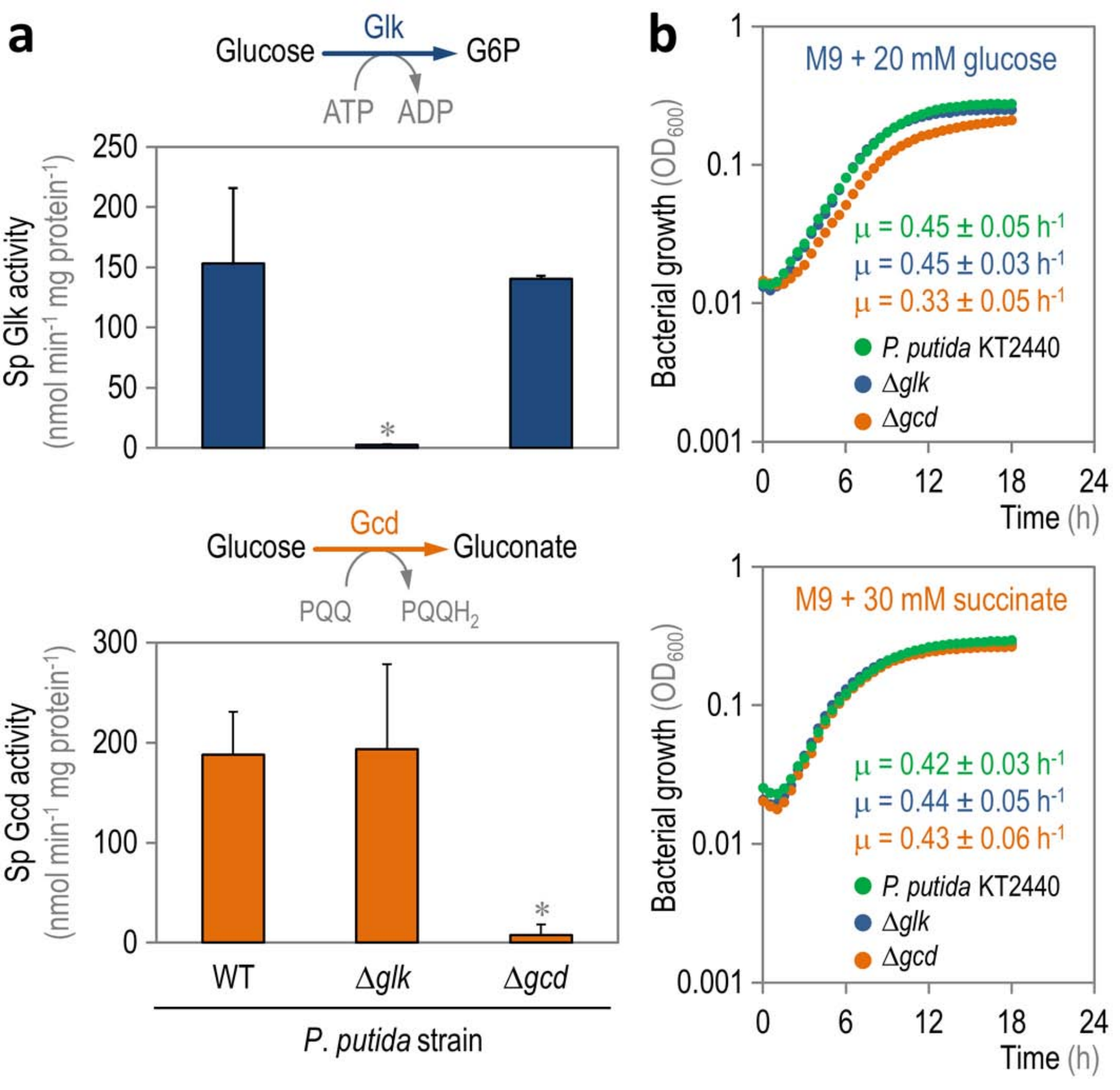
a
Glucose
Glk
G6P
ATP
ADP
Sp Glk activity
(nmol min-1 mg protein-1)
250
200
150
100
50
0
*
Glucose
Gcd
Gluconate
PQQ
PQQH2
Sp Gcd activity
(nmol min-1 mg protein-1)
300
200
100
0
*
WT
Δglk
Δgcd
P. putida strain
b
M9 + 20 mM glucose
Bacterial growth (OD600)
1
0.1
0.01
0.001
μ = 0.45 ± 0.05 h-1
μ = 0.45 ± 0.03 h-1
μ = 0.33 ± 0.05 h-1
P. putida KT2440
Δglk
Δgcd
0
6
12
18
24
Time (h)
M9 + 30 mM succinate
Bacterial growth (OD600)
1
0.1
0.01
0.001
μ = 0.42 ± 0.03 h-1
μ = 0.44 ± 0.05 h-1
μ = 0.43 ± 0.06 h-1
P. putida KT2440
Δglk
Δgcd
0
6
12
18
24
Time (h)

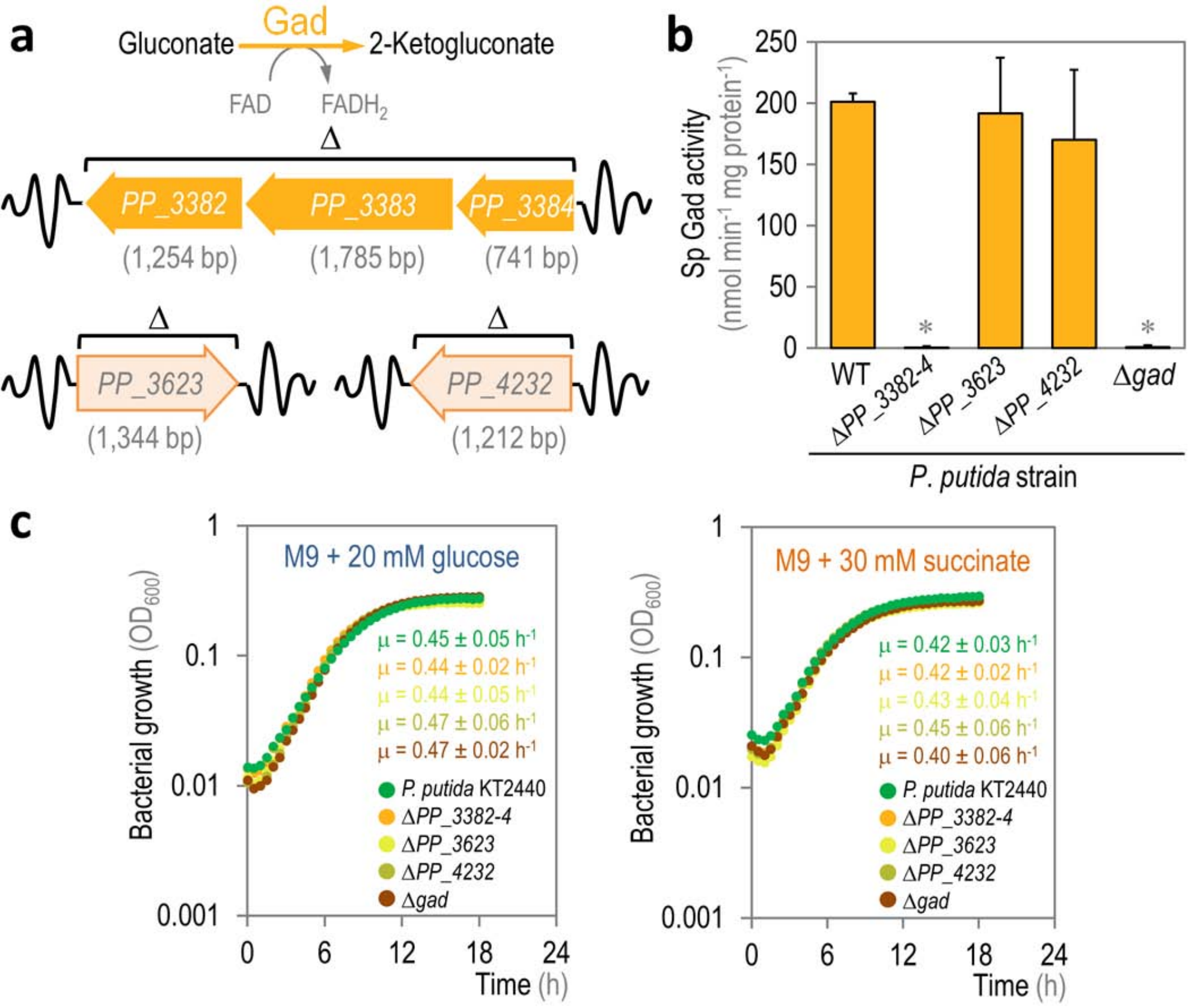
a
Gluconate
Gad
2-Ketogluconate
FAD
FADH2
Δ
PP_3382
PP_3383
PP_3384
(1,254 bp)
(1,785 bp)
(741 bp)
Δ
Δ
PP_3623
PP_4232
(1,344 bp)
(1,212 bp)
b
Sp Gad activity
(nmol min-1 mg protein-1)
250
200
150
100
50
0
*
*
WT
ΔPP_3382-4
ΔPP_3623
ΔPP_4232
Δgad
P. putida strain
c
M9 + 20 mM glucose
Bacterial growth (OD600)
1
0.1
0.01
0.001
μ = 0.45 ± 0.05 h-1
μ = 0.44 ± 0.02 h-1
μ = 0.44 ± 0.05 h-1
μ = 0.47 ± 0.06 h-1
μ = 0.47 ± 0.02 h-1
P. putida KT2440
ΔPP_3382-4
ΔPP_3623
ΔPP_4232
Δgad
0
6
12
18
24
Time (h)
M9 + 30 mM succinate
Bacterial growth (OD600)
1
0.1
0.01
0.001
μ = 0.42 ± 0.03 h-1
μ = 0.42 ± 0.02 h-1
μ = 0.43 ± 0.04 h-1
μ = 0.45 ± 0.06 h-1
μ = 0.40 ± 0.06 h-1
P. putida KT2440
ΔPP_3382-4
ΔPP_3623
ΔPP_4232
Δgad
0
6
12
18
24
Time (h)

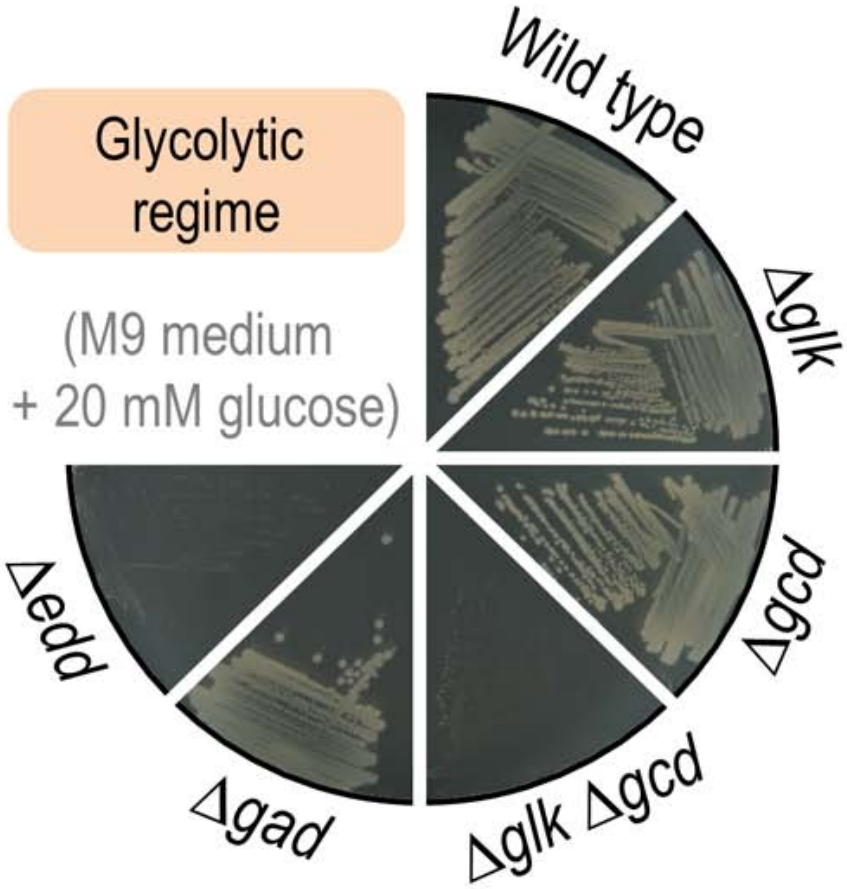

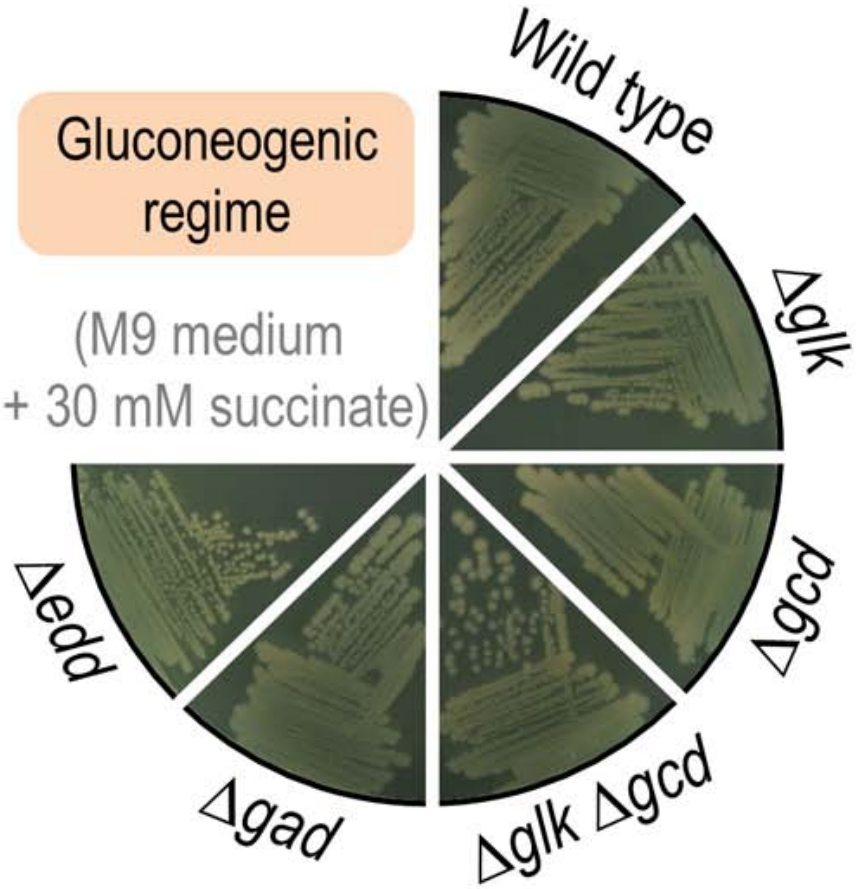

Strain	M9 medium +	
	20 mM glucose	30 mM succinate
P. putida KT2440	+ (100)	+ (100)
P. putida Δ*glk*	+ (100)	+ (100)
P. putida Δ*gcd*	+ (73)	+ (100)
P. putida Δ*glk* Δ*gcd*	–	+ (93)
P. putida Δ*gad*	+ (100)	+ (100)
P. putida Δ*edd*	–	+ (86)

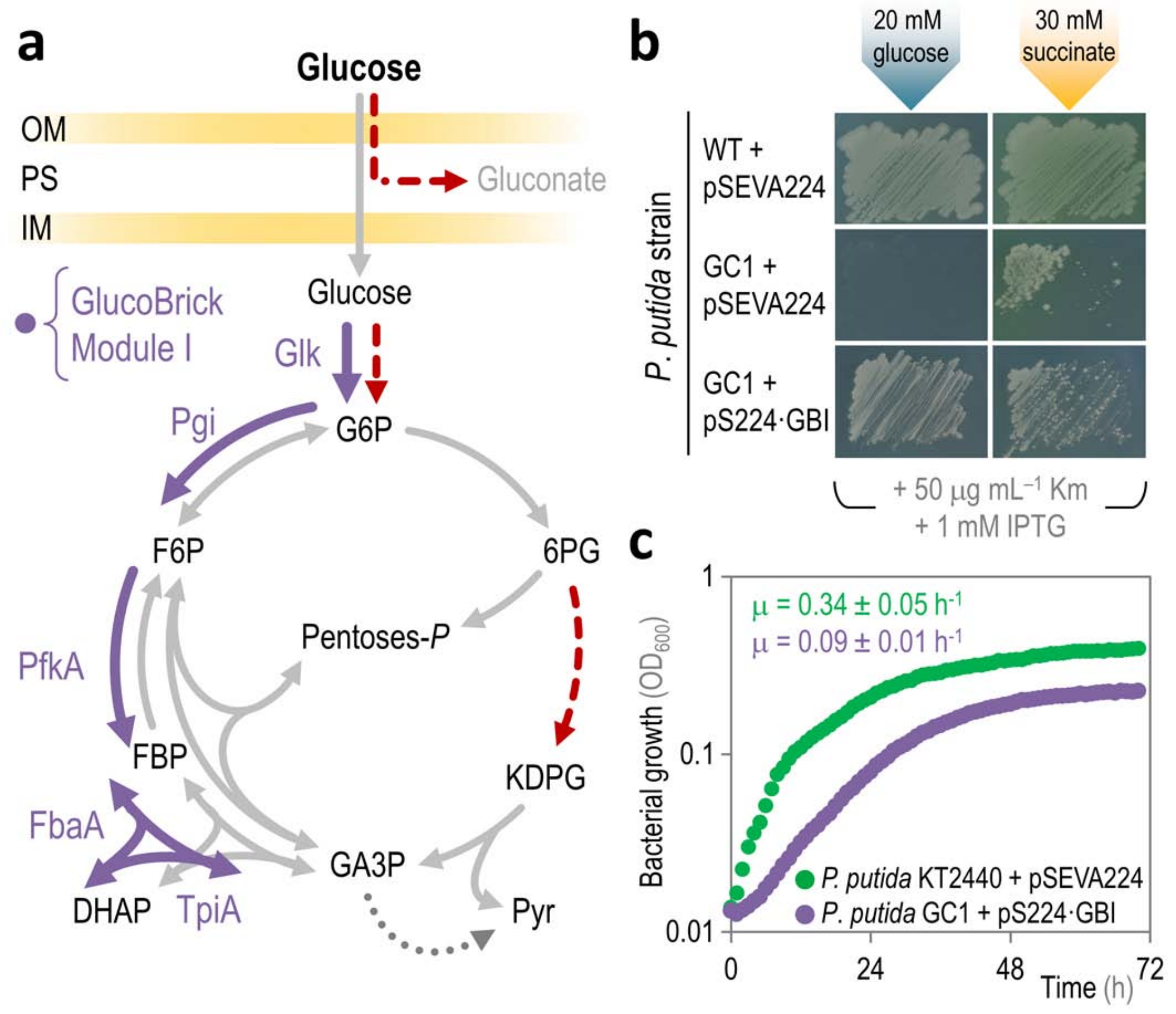
a
Glucose
OM
PS
IM
Gluconate
Glucose
GlucoBrick
Module I
Glk
Pgi
G6P
F6P
6PG
Pentoses-P
PfkA
FBP
KDPG
FbaA
GA3P
DHAP
TpiA
Pyr
b
20 mM glucose
30 mM succinate
P. putida strain
WT + pSEVA224
GC1 + pSEVA224
GC1 + pS224·GBI
+ 50 μg mL⁻¹ Km
+ 1 mM IPTG
c
μ = 0.34 ± 0.05 h⁻¹
μ = 0.09 ± 0.01 h⁻¹
Bacterial growth (OD600)
1
0.1
0.01
0
24
48
72
Time (h)
P. putida KT2440 + pSEVA224
P. putida GC1 + pS224·GBI

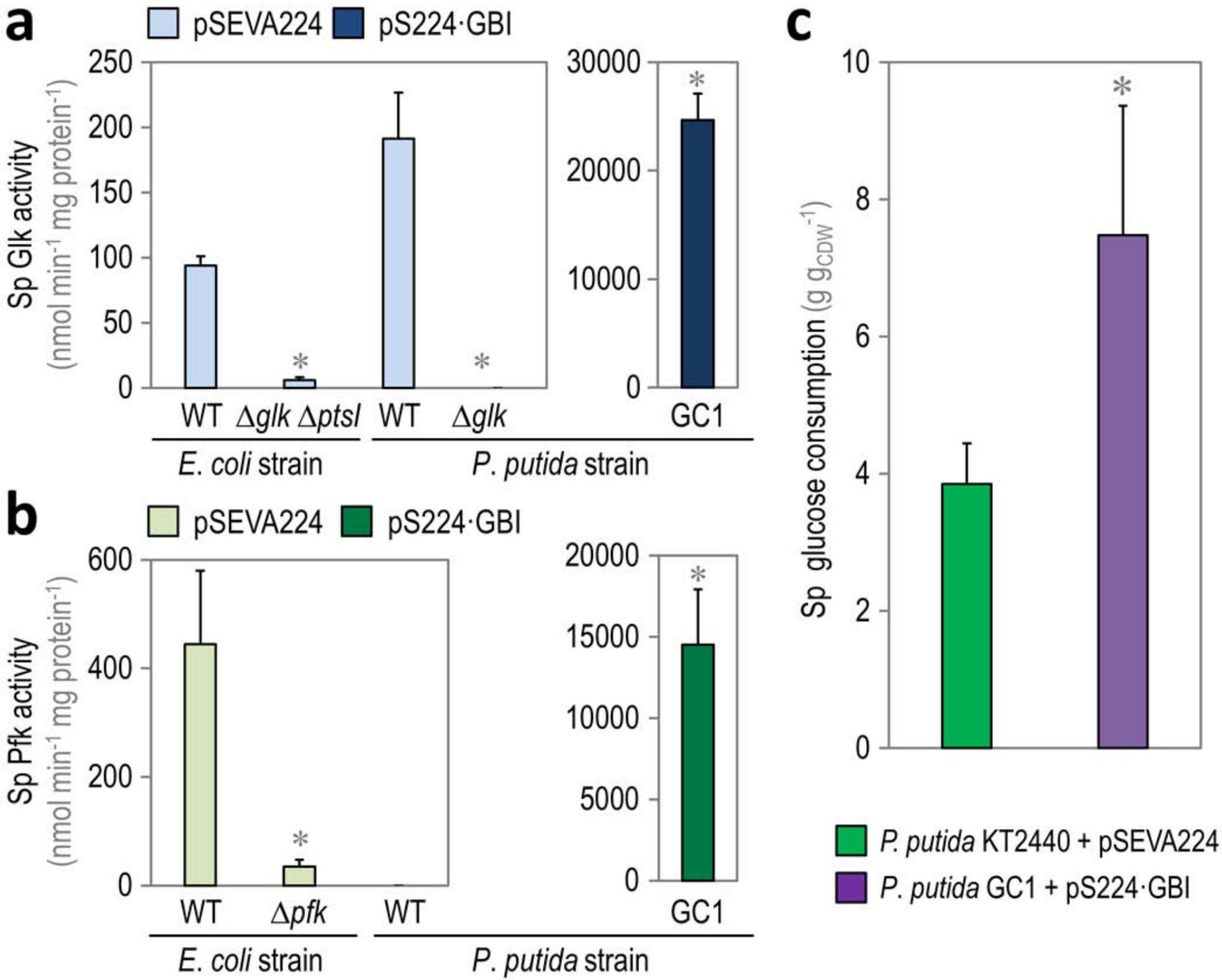
a
pSEVA224
pS224·GBI
Sp Glk activity
(nmol min-1 mg protein-1)
250
200
150
100
50
0
30000
20000
10000
0
*
WT
Δglk Δptsl
WT
Δglk
GC1
E. coli strain
P. putida strain
b
pSEVA224
pS224·GBI
Sp Pfk activity
(nmol min-1 mg protein-1)
600
400
200
0
20000
15000
10000
5000
0
WT
Δpfk
WT
GC1
E. coli strain
P. putida strain
c
Sp glucose consumption (g gCDW-1)
10
8
6
4
2
0
P. putida KT2440 + pSEVA224
P. putida GC1 + pS224·GBI

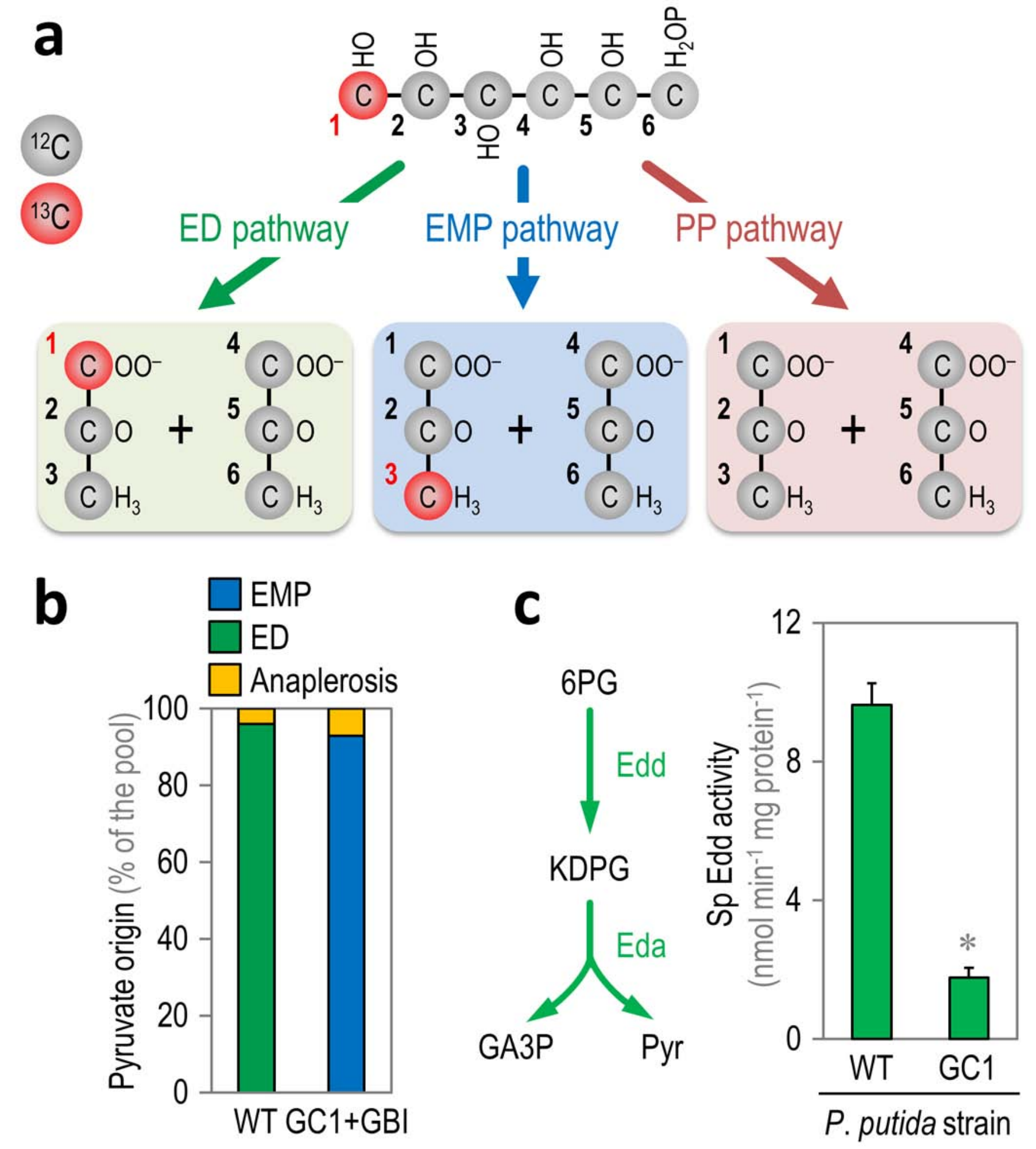
a
12C
13C
HO
OH
OH
OH
H2OP
C
1
2
3
4
5
6
ED pathway
EMP pathway
PP pathway
COO−
CO
CH3
b
EMP
ED
Anaplerosis
Pyruvate origin (% of the pool)
100
80
60
40
20
0
WT
GC1+GBI
c
6PG
Edd
KDPG
Eda
GA3P
Pyr
Sp Edd activity
(nmol min-1 mg protein-1)
12
8
4
0
*
WT
GC1
P. putida strain

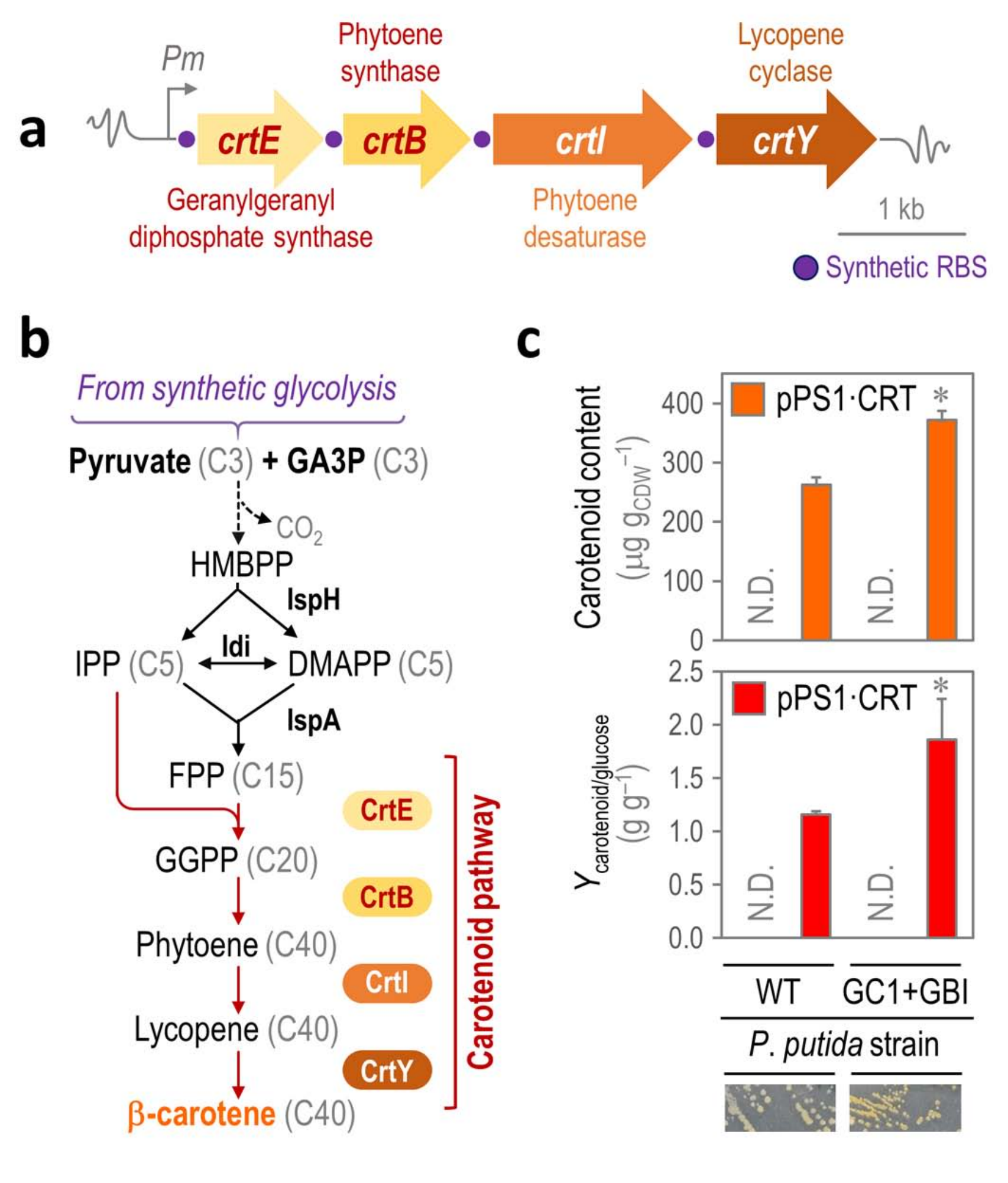
a
Pm
crtE
crtB
crtI
crtY
Phytoene synthase
Lycopene cyclase
Geranylgeranyl diphosphate synthase
Phytoene desaturase
1 kb
Synthetic RBS
b
From synthetic glycolysis
Pyruvate (C3) + GA3P (C3)
CO2
HMBPP
IspH
Idi
IPP (C5)
DMAPP (C5)
IspA
FPP (C15)
CrtE
GGPP (C20)
CrtB
Phytoene (C40)
CrtI
Lycopene (C40)
CrtY
β-carotene (C40)
Carotenoid pathway
c
Carotenoid content
(μg gCDW−1)
pPS1·CRT
*
N.D.
N.D.
Ycarotenoid/glucose
(g g−1)
WT
GC1+GBI
P. putida strain

Supplementary Material

Functional implementation of a linear glycolysis for sugar catabolism in *Pseudomonas putida*

by

Alberto Sánchez-Pascuala, Lorena Fernández-Cabezón, Víctor de Lorenzo, and Pablo I. Nikel

SUPPLEMENTARY METHODS

Construction of mutant *Pseudomonas putida* strains. Clean *P. putida* knock-out mutants were obtained following the protocol described by Martínez-García and de Lorenzo (2011). The method is based on the use of the suicide pEMG vector (**Table S1**), containing flanking regions upstream and downstream of the target gene(s) amplified by PCR using chromosomal DNA from strain KT2440 as the template. The oligonucleotides employed to amplify these *ca*. 500-bp long flanking regions (termed *TS1*, upstream; and *TS2*, downstream) are listed in **Table S2**. A 1-kbp amplification product (i.e. spanning the TS1-TS2 regions that flank the target gene or group of genes, indicated with "*x*" in the primer names) were obtained using the two individual 500-bp amplicons as the template and external oligonucleotides (i.e. *x*-TS1F and *x*-TS2R) by splicing-by-overlap extension (*SOEing*) PCR (Horton, 1995; Nikel and de Lorenzo, 2013). The TS1-TS2 DNA modules were digested with *Eco*RI and *Bam*HI (except for the cases indicated in **Table S2**), cloned into the I-*Sce*I–bearing pEMG vector digested with the same enzymes [giving rise to plasmid(s) pEMGΔ*x*, **Table S1**] and verified by enzyme restriction and DNA sequencing. The resulting pEMGΔ*x* vectors were electroporated in *P. putida* KT2440 (and derivatives thereof) to force cointegration events (as pEMG-derived plasmids lack a compatible origin of replication for *Pseudomonas* species). Merodiploids were selected by plating bacteria in lysogeny broth (LB) medium plates containing kanamycin (Km) and individual clones were checked by PCR using oligonucleotides *x*-TS1F and *x*-TS2R. Once a suitable cointegration event was obtained, the selected bacterial clone was transformed with plasmid pSW-I and selected in LB medium plates containing ampicillin (Ap). In order to facilitate the recombination process (mediated by the I-*Sce*I endonuclease) that allows for the deletion event, the strains were incubated for 6 h in 5 ml of LB medium containing 500 μg ml^{-1} Ap and 15 mM sodium 3-methylbenzonate (3-*m*Bz). The resulting cultures were plated onto LB medium plates to obtain individual colonies, which were re-streaked onto LB medium with or without Km to check for the loss of the cointegrated plasmid. Km-sensitive clones were analyzed by colony PCR (using the pair of oligonucleotides *x*-TS1F and *x*-TS2R) to distinguish between events leading to either deletion of the intended region or revertant [i.e. wild-type genotype]. As a final step, the pSW-I plasmid was eliminated from the strains after several consecutive passes in liquid LB medium. In order to verify the elimination of plasmid pSW-I, all the candidates were plated onto LB medium plates with 500 μg ml^{-1} Ap and checked by PCR using the oligonucleotides pSW-F and pSW-R.

Preparation of bacterial cell-free extracts. Cell-free extracts of *Escherichia coli* and *P. putida* were obtained by a modification of published protocols (Chavarría et al., 2016; Nikel et al., 2014). Enzyme activity determinations were carried out in cell-free extracts obtained from bacterial cultures harvested during the mid-exponential phase of growth [i.e. corresponding to an optical density measured at 600 nm (OD_{600}) of ca. 0.5]. Cell-free extracts were obtained from 50 ml of culture broth (in 250-ml Erlenmeyer flasks). Biomass was collected by centrifuging the cultures at 4,000 r.p.m. for 15 min at 4ºC. Cell pellets were washed twice with 25 ml of pre-cooled 67 mM potassium phosphate buffer (pH = 7.1) at 4ºC. From this step onwards, the protocol followed to obtain cell-free extracts was modified depending on the location of the enzyme (i.e. membrane-bound or cytoplasm). For enzymes located in or associated with the cell membrane (e.g. Gcd and Gad), the resulting pellets were suspended in 2-ml Eppendorf tubes with the appropriate volume of pre-cooled 60 mM glycylglycine buffer (pH = 7.1) to obtain a cell density of 0.2 g of cells (wet weight) per milliliter of buffer. The suspensions were sonicated in seven 30-s intervals separated by 1.5 min rests in ice to avoid heating of the sample (18-20 kHz, 1.0-1.5 A). At this point, the mixtures were centrifuged at 13,000 r.p.m. for 30 min at 4ºC to remove insoluble cell debris. The cell-free extracts were stored at –20ºC until use.

In the case of cytoplasmic enzymes, pellets were washed with 67 mM potassium phosphate buffer obtained as explained above, and bacteria were resuspended in 1 ml of the same buffer and centrifuged in 2-ml Eppendorf tubes at 8,000 r.p.m. for 10 min at 4ºC. After carefully removing the supernatant, the cell wet weight was obtained for each pellet in order to calculate the volume of reagents needed for protein extraction using the Novagen BugBuster™ protocol (EMD Millipore Corp., Billerica, MA, USA). Pellets and cell-free extracts were kept on ice throughout the whole procedure. Bacterial lysis was achieved by adding 5 ml of BugBuster™ Protein Extraction Reagent per gram of bacterial cell paste. Afterwards, 1 μl of Lysonase™ Bioprocessing Reagent was added per 1 ml of BugBuster™ Protein Extraction Reagent used for re-suspension of the cells. Bacteria were lysed by shaking for 20 min at room temperature in a Rotamax 120 orbital shaker (Heidolph Instruments GmbH & Co. KG, Schwabach, Germany) at 150 r.p.m. The insoluble cell debris was removed by centrifugation at 13,000 r.p.m. for 20 min at 4ºC and the supernatants (i.e. cell-free extracts) were stored at –20ºC until use.

***In vitro* enzymatic assays.** In order to determine the activity of two key glycolytic enzymes (Glk and Pfk), the *in vitro* assays were carried out at 30ºC when using cell-free extracts from *P. putida* or at 37ºC when using cell-free extracts from *E. coli*. The remaining activities were measured at 25ºC as indicated by Sigma-Aldrich Co. (St. Louis, MO, USA) in the corresponding enzymatic assay protocols or by following previously described procedures (Ng and Dawes, 1973; Nikel et al., 2014). All the enzymes were assessed under the optimal reported conditions for pH, substrate, and cofactor concentration (Chavarría et al., 2013; Nikel and Chavarría, 2016; Nikel et al., 2014; 2015). *In vitro* assays were conducted in Nunc™ MicroWell™ 96-well microplates (Thermo Fisher Scientific Inc., Waltham, MA, USA) in a SpectraMax™ M2e multi-mode microplate reader (Molecular Devices LLC, Sunnyvale, CA, USA). All the specific enzyme activities are reported as nmol of substrate converted min^{-1} mg of $protein^{-1}$.

Protein concentration in cell-free extracts was assessed using the Bradford Protein Assay (Bio-Rad Laboratories Inc., Hercules, CA, USA) (Bradford, 1976). All the accessory enzymes (with the exceptions indicated below) were from *Saccharomyces cerevisiae* and they were purchased from Sigma-Aldrich Co. (St. Louis, MO, USA). An extinction coefficient [$\varepsilon_{NAD(P)/H}$] of 6.22 mM^{-1} cm^{-1}, representing the difference between the extinction coefficients of NAD(P)H and $NAD(P)^+$. In the case of dichlorophenolindophenol (DCPIP), the extinction coefficients were experimentally determined to be 4.1 mM^{-1} cm^{-1} at 600 nm (pH = 5.5) and 9.1 mM^{-1} cm^{-1} at 576 nm (pH = 5.5). The limit of detection for all the enzymatic assays was consistently below 2-5 nmol min^{-1} mg of $protein^{-1}$. Specific protocols used for the determinations are detailed below.

Edd. *6-Phosphogluconate dehydratase* (EC 4.2.1.12). The Edd activity was assayed in a two-step reaction protocol by a modification of previously published methods (Baumann and Baumann, 1975; Ponce et al., 2005; Vicente and Cánovas, 1973). The assay mixture contained, in a final volume of 0.1 ml, 50 mM Tris·HCl buffer (pH = 7.5), 10 mM $MgCl_2$, 10 μM gluconate-6-*P*, and an appropriate dilution of the cell-free extract. This mixture was incubated for 5 min at room temperature and diluted with the same reaction buffer up to 2 ml. The mixture was heated for 2 min at 95ºC and centrifuged at 14,000 r.p.m. during 10 min at room temperature. The supernatant solution was assayed for pyruvate formation by using a mixture that contained 20 μl of the supernatant and 180 μl of a solution containing 50 mM Tris·HCl buffer (pH = 7.5), 10 mM $MgCl_2$, 1mM EDTA, 0.1 mM NADH, and 0.5 units of L-lactate dehydrogenase from bovine heart. The decrease in absorbance at 340 nm (A_{340}) was measured during the assay at 37ºC.

Gad. *Gluconate 2-dehydrogenase* (EC 1.1.99.3). The reaction mixture contained 40 μl of 100 mM sodium acetate buffer (pH = 5.5), 16.7 μl of 75 mM sodium gluconate, 6.7 μl of 15 mM KCN, 33.2 μl of DCPIP (0.5 mg ml^{-1}), 96.7 μl of water, and 6.7 μl of cell-free extract (or an appropriate dilution in 100 mM sodium acetate buffer pH = 5.5). The decrease in absorbance at 576 nm (A_{576}) was measured during the assay.

Gcd. *Glucose dehydrogenase* (EC 1.1.1.47). The reaction mixture contained 66.7 μl of 100 mM sodium acetate buffer (pH = 5.5), 36.7 μl of 75 mM glucose, 6.7 μl of 15 mM KCN, 13.2 μl of DCPIP (0.5 mg ml^{-1}), 70 μl of water, and 6.7 μl of cell-free extract (or an appropriate dilution in 100 mM sodium acetate buffer pH = 5.5). The decrease in absorbance at 600 nm (A_{600}) was measured during the assay.

Glk. *ATP–D-Hexose 6-phosphotransferase* or *glucokinase* (EC 2.7.1.1). The reaction mixture contained 67 μl of 120 mM Tris·HCl buffer (pH = 8.2), 26 μl of 500 mM glucose, 8 μl of 250 mM $MgCl_2$, 53 μl of 36 mM ATP, 10 μl of 20 mM $NADP^+$, 13 μl of glucose-6-*P* dehydrogenase (15 units ml^{-1}), 18 μl of water, and 5 μl of cell-free extract (or an appropriate dilution in 67 mM potassium phosphate buffer, pH = 7.1). The increase in A_{340} was measured during the assay.

Pfk. *6-Phosphofructo-1-kinase* (EC 2.7.1.11). The reaction mixture contained 20 μl of 1 M Tris·HCl buffer (pH = 7.5), 2 μl of 100 mM fructose-6-*P*, 8 μl of 250 mM $MgCl_2$, 4 μl of 100 mM NH_4Cl, 4 μl of 10 mM NADH, 6 μl of 36 mM ATP, 4 μl of fructose-1,6-P_2 aldolase (50 units ml^{-1}), 1.5 μl of triosephosphate isomerase (500 units ml^{-1}), 1.5 μl of glycerol-3-*P* dehydrogenase from rabbit muscle (170 units ml^{-1}), 144 μl of water, and 5 μl of cell-free extract (or an appropriate dilution in 67 mM potassium phosphate buffer, pH = 7.1). The decrease in A_{340} was measured during the assay.

Table S1. Plasmids used in this study.

Plasmids	Relevant characteristics[a]	Reference or source
pKD46	Ap^R; helper plasmid expressing the λ-Red recombination functions	Datsenko and Wanner (2000)
pCP20	Ap^R Cm^R; helper plasmid used for excision of *FRT-aphA-FRT* (Km^R), *Saccharomyces cerevisiae FLP* λ*c*I857 λP_R *repA*(Ts)	Cherepanov and Wackernagel (1995)
pEMG	Km^R; *oriV*(R6K), vector used for deletions, *lacZ*α with two flanking I-*Sce*I target sites	Martínez-García and de Lorenzo (2011)
pEMGΔ*glk*	Km^R; pEMG derivative bearing a 1.0-kb TS1-TS2 *Eco*RI-*Bam*HI insert for deletion of the *glk* gene of *P. putida* KT2440	Sánchez-Pascuala et al. (2017)
pEMGΔ*gcd*	Km^R; pEMG derivative bearing a 1.0-kb TS1-TS2 *Eco*RI-*Bam*HI insert for deletion of the *gcd* gene of *P. putida* KT2440	This study
pEMGΔ *PP_3382-4*	Km^R; pEMG derivative bearing a 1.0-kb TS1-TS2 *Eco*RI-*Bam*HI insert for deletion of the group of genes *PP_3382*, *PP_3383* and *PP_3384* of *P. putida* KT2440	This study
pEMGΔ *PP_3623*	Km^R; pEMG derivative bearing a 1.0-kb TS1-TS2 *Eco*RI-*Bam*HI insert for deletion of the *PP_3623* gene of *P. putida* KT2440	This study
pEMGΔ *PP_4232*	Km^R; pEMG derivative bearing a 1.0-kb TS1-TS2 *Sac*I-*Bam*HI insert for deletion of the *PP_4232* gene of *P. putida* KT2440	This study
pEMGΔ*edd*	Km^R; pEMG derivative bearing a 1.0-kb TS1-TS2 *Eco*RI-*Bam*HI insert for deletion of the *edd* gene of *P. putida* KT2440	This study
pEMGΔ*edd* Δ*glk*	Km^R; pEMG derivative bearing a 1.0-kb TS1-TS2 *Eco*RI-*Bam*HI insert for deletion of the *edd* gene of *P. putida* KT2440 Δ*glk*	This study
pSW-I[b]	Ap^R; *oriV*(RK2), *xylS*, *Pm*→I-*Sce*I, transcriptional fusion of the gene encoding I-*Sce*I to the *Pm* promoter	Wong and Mekalanos (2000)
pSEVA224	Km^R; standard SEVA expression vector, *oriV*(RK2) $lacI^Q$, P_{trc}	Silva-Rocha et al. (2013)
pS224·GBI	Km^R; pSEVA224 derivative bearing Module I as an *Avr*II-*Bam*HI insert	Sánchez-Pascuala et al. (2017)
pPS1	Gm^R; pSEVA441 derivative adapted for easy *USER* cloning, *oriV*(pBBR1), *xylS-Pm*	Calero et al. (2016)
pSEVA13-sl3T7-*crtEBIY*	Ap^R; *oriV*(pBBR1), P_{T7}→*crtEBIY*, used as a template to amplify the genes encoding the β-carotene biosynthetic pathway from *Pantoea ananatis*	Kim et al. (2016)
pPS1·CRT	Gm^R; pPS1 derivative, *xylS*, *Pm*→*crtEBIY*	This study

[a] Antibiotic markers: *Ap*, ampicillin; *Cm*, chloramphenicol; *Gm*, gentamicin; and *Km*, kanamycin. Ts, temperature-sensitive origin of replication.

[b] This plasmid is the same as pSW(I-*Sce*I) described by Wong and Mekalanos (2000), renamed here as pSW-I for simplicity.

Table S2. Oligonucleotides used in this study.

Name	Sequence (5' → 3')[a]	Tm (ºC)	Use
PP_1011-TS1F-*Eco*RI	G**GA ATT C**GA GGC CCC GGC GCG GGT GTT CCA GGA CCA G	88	Construction of *P. putida* Δ*glk*
PP_1011-TS1R	*CAT CGG GGC CGC AAA GCG CCC CCC TCA GTG* GTG CTT CAT TTG AGG TGC TCC AGG GCC GAG	92	
PP_1011-TS2F	*CAC TGA GGG GGG CGC TTT GCG GCC CCG ATG*	86	
PP_1011-TS2R-*Bam*HI	CG**G GAT CC**C GCC AGT CGT CGA AGG CCA GCA CGG CGT TG	88	
PP_1444-TS1F-*Eco*RI	G**GA ATT C**GC GGC AGT GCC GAG GTG TCG AAG TGG CGG TGG	86	Construction of *P. putida* Δ*gcd*
PP_1444-TS1R	*GGC CTG AAG ATC CAG AGC AGT TTC TAA CCC* GCG ACA CCG CTC CCG CAG GCT CAA CCC TGA GG	89	
PP_1444-TS2F	*GGG TTA GAA ACT GCT CTG GAT CTT CAG GCC*	74	
PP_1444-TS2R-*Bam*HI	CG**G GAT CC**G TCA GCC GGC CGC CCT CAG CGG CGC CGC CT	95	
PP_3382-4-TS1F-*Eco*RI	G**GA ATT C**GT CGT CAG TAA AGG ACG TGA ACG ACT GGA C	76	Construction of *P. putida* Δ*PP_3382-4*
PP_3382-4-TS1R	*CAA GGC CGC CCC ACA GCC GAT GAG GAT TCG* CGT GTT TTT CAG CGC CCT CGC CCG TAG GAG	91	
PP_3382-4-TS2F	*GGG TTA GAA ACT GCT CTG GAT CTT CAG GCC*	74	
PP_3382-4-TS2R-*Bam*HI	CG**G GAT CC**G TCA GCC GGC CGC CCT CAG CGG CGC CGC CT	95	
PP_3623-TS1F-*Eco*RI	**GA ATT C**TT GTC CGG CGG CTG GAA GCG CGG ACC GTT C	85	Construction of *P. putida* Δ*PP_3623*
PP_3623-TS1R	*CAG CCT CGC GTC GGT ACA TGT GCC ACT CCA* AGG CGT CCC TTG TGC GAT CAG CTG AAG GTG	89	
PP_3623-TS2F	*TGG AGT GGC ACA TGT ACC GAC GCG AGG CTG*	81	
PP_3623-TS2R-*Bam*HI	CG**G GAT CC**T CAT CTG GGT GCG CCA GGA CAA TGC CTT TG	83	
PP_4232-TS1F-*Sac*I	C**GA GCT C**GC CGA CAC GCA AGC GCA CCC GGG CAT TTT C	87	Construction of *P. putida* Δ*PP_4232*
PP_4232-TS1R	*CGA TCT CGG CCT GGT CAA GGA GGG TTG AAC* AGC GTG CAG CAT CTC GAT CTA CAG GTG ATC	85	
PP_4232-TS2F	*GTT CAA CCC TCC TTG ACC AGG CCG AGA TCG*	78	
PP_4232-TS2R-*Bam*HI	CG**G GAT CC**C CGG TCG GGC CGG TCG AGG TTC CCG CGG AC	92	

PP_1010-TS1F-*Eco*RI	G**GA ATT C**GC ACT GAC CGC GAT ACG GTC	75	Construction of *P. putida* ∆*edd*
PP_1010-TS1R	*CAC CAA CCA GCA GGT GCT TCA T*GT ACT GGA CTC CAG GCT AAT TG	80	
PP_1010-TS2F	*ATG AAG CAC CTG CTG GTT GGT G*	71	
PP_1010-TS2R-*Bam*HI	CG**G GAT CC**C CTA CCG GCA GGT CAA CAT G	79	
PP_1010(∆*glk*)-TS1R	*GCA AAG CGC CCC CCT CAG TG*G TAC TGG ACT CCA GGC TAA TTG	83	Used in combination with *PP_1010*-TS1F-*Eco*RI and *PP_1010*-TS2R-*Bam*HI to remove *edd* in *P. putida* ∆*glk*
PP_1010(∆*glk*)-TS2F	*CAC TGA GGG GGG CGC TTT GC*	75	
pfkA·*fbaA*-Check-F	GAA AGG TAA AAA ACA CGC GAT C	59	Screening of recombinants carrying Module I[b]
pfkA·*fbaA*-Check-R	ACG CTG CGA TGG TGA AAC	59	
crtEBIY-UC-F	AAG GAG AUA TAC CTA TGA CGG TCT GCG	65	Construction of plasmid pPS1·CRT
crtEBIY-UC-R	ACG ATG AGU CGT CAT AAT GGC TTG CAA	67	
pPS1*crtEBIY*-UC-F	ACT CAT CGU TAA GAA TTC GAG CTC GGT ACC CG	69	
pPS1*crtEBIY*-UC-R	ATC TCC TUC CTA GGG CGA TCG CCT CAG C	71	

[a] Bold letters indicate recognition site for the restriction enzymes and the complementary sequences used in splicing-by-overlap extension (*SOEing*) PCR amplifications (Horton, 1995; Nikel and de Lorenzo, 2013) are shown in italics. Oligonucleotides containing *U* residues, added for *USER* cloning purposes (Nour-Eldin et al., 2010), are indicated with the identifier 'UC'.

[b] A PCR amplification using these oligonucleotides yields a 1,015-bp amplicon in the junction of the *pfkA* and *fbaA* genes.

REFERENCES

Baumann, P., Baumann, L., 1975. Catabolism of D-fructose and D-ribose by *Pseudomonas doudoroffi* – I. Physiological studies and mutant analysis. Arch. Microbiol. 105**,** 225-240.

Bradford, M. M., 1976. A rapid and sensitive method for the quantitation of microgram quantities of protein utilizing the principle of protein-dye binding. Anal. Biochem. 72**,** 248-254.

Calero, P., Jensen, S. I., Nielsen, A. T., 2016. Broad-host-range *ProUSER* vectors enable fast characterization of inducible promoters and optimization of *p*-coumaric acid production in *Pseudomonas putida* KT2440. ACS Synth Biol. 5, 741-753.

Chavarría, M., Goñi-Moreno, A., de Lorenzo, V., Nikel, P. I., 2016. A metabolic widget adjusts the phosphoenolpyruvate-dependent fructose influx in *Pseudomonas putida*. mSystems. 1**,** e00154-16.

Chavarría, M., Nikel, P. I., Pérez-Pantoja, D., de Lorenzo, V., 2013. The Entner-Doudoroff pathway empowers *Pseudomonas putida* KT2440 with a high tolerance to oxidative stress. Environ. Microbiol. 15**,** 1772-1785.

Cherepanov, P. P., Wackernagel, W., 1995. Gene disruption in *Escherichia coli*: Tc^R and Km^R cassettes with the option of Flp-catalyzed excision of the antibiotic-resistance determinant. Gene. 158**,** 9-14.

Datsenko, K. A., Wanner, B. L., 2000. One-step inactivation of chromosomal genes in *Escherichia coli* K-12 using PCR products. Proc. Natl. Acad. Sci. USA. 97**,** 6640-6645.

Horton, R. M., 1995. PCR-mediated recombination and mutagenesis: *SOEing* together tailor-made genes. Mol. Biotechnol. 3**,** 93-99.

Kim, S. H., Cavaleiro, A. M., Rennig, M., Nørholm, M. H., 2016. *SEVA Linkers*: A versatile and automatable DNA backbone exchange standard for Synthetic Biology. ACS Synth. Biol. 5, 1177-1181.

Martínez-García, E., de Lorenzo, V., 2011. Engineering multiple genomic deletions in Gram-negative bacteria: Analysis of the multi-resistant antibiotic profile of *Pseudomonas putida* KT2440. Environ. Microbiol. 13**,** 2702-2716.

Ng, F. M., Dawes, E. A., 1973. Chemostat studies on the regulation of glucose metabolism in *Pseudomonas aeruginosa* by citrate. Biochem. J. 132**,** 129-140.

Nikel, P. I., de Lorenzo, V., 2013. Implantation of unmarked regulatory and metabolic modules in Gram-negative bacteria with specialised mini-transposon delivery vectors. J. Biotechnol. 163**,** 143-154.

Nikel, P. I., Kim, J., de Lorenzo, V., 2014. Metabolic and regulatory rearrangements underlying glycerol metabolism in *Pseudomonas putida* KT2440. Environ. Microbiol. 16**,** 239-254.

Nikel, P. I., Chavarría, M., Fuhrer, T., Sauer, U., de Lorenzo, V., 2015. *Pseudomonas putida* KT2440 strain metabolizes glucose through a cycle formed by enzymes of the Entner-Doudoroff, Embden-Meyerhof-Parnas, and pentose phosphate pathways. J. Biol. Chem. 290**,** 25920-25932.

Nikel, P. I., Chavarría, M., 2016. Quantitative physiology approaches to understand and optimize reducing power availability in environmental bacteria. In: McGenity, T. J., Timmis, K. N., Nogales-Fernández, B. (Eds.), Hydrocarbon and Lipid Microbiology Protocols – Synthetic and Systems Biology – Tools. Humana Press, Heidelberg, Germany, pp. 39-70.

Nour-Eldin, H. H., Geu-Flores, F., Halkier, B. A., 2010. *USER* cloning and *USER* fusion: The ideal cloning techniques for small and big laboratories. Methods Mol. Biol. 643, 185-200.

Ponce, E., García, M., Muñoz, M. E., 2005. Participation of the Entner-Doudoroff pathway in *Escherichia coli* strains with an inactive phosphotransferase system (PTS^- Glc^+) in gluconate and glucose batch cultures. Can. J. Microbiol. 51**,** 975-982.

Sánchez-Pascuala, A., de Lorenzo, V., Nikel, P. I., 2017. Refactoring the Embden-Meyerhof-Parnas pathway as a whole of portable GlucoBricks for implantation of glycolytic modules in Gram-negative bacteria. ACS Synth Biol. 6**,** 793-805.

Silva-Rocha, R., Martínez-García, E., Calles, B., Chavarría, M., Arce-Rodríguez, A., de las Heras, A., Páez-Espino, A. D., Durante-Rodríguez, G., Kim, J., Nikel, P. I., Platero, R., de Lorenzo, V., 2013. The *Standard European Vector Architecture* (SEVA): A coherent platform for the analysis and deployment of complex prokaryotic phenotypes. Nucleic Acids Res. 41**,** D666-D675.

Vicente, M., Cánovas, J. L., 1973. Glucolysis in *Pseudomonas putida*: Physiological role of alternative routes from the analysis of defective mutants. J. Bacteriol. 116**,** 908-914.

Wong, S. M., Mekalanos, J. J., 2000. Genetic footprinting with *mariner*-based transposition in *Pseudomonas aeruginosa*. Proc. Natl. Acad. Sci. USA. 97**,** 10191-10196.